Atmos. Chem. Phys., 16, 13753–13772, 2016
www.atmos-chem-phys.net/16/13753/2016/
doi:10.5194/acp-16-13753-2016

Atmospheric Chemistry and Physics Open Access EGU

Estimating contributions from biomass burning, fossil fuel combustion, and biogenic carbon to carbonaceous aerosols in the Valley of Chamonix: a dual approach based on radiocarbon and levoglucosan

Lise Bonvalot[1], Thibaut Tuna[1], Yoann Fagault[1], Jean-Luc Jaffrezo[2], Véronique Jacob[2], Florie Chevrier[2,3], and Edouard Bard[1]

[1]CEREGE, Aix-Marseille University, CNRS, IRD, Collège de France, Technopôle de l'Arbois, BP 80, 13545 Aix-en-Provence, France
[2]Université Grenoble Alpes/CNRS, LGGE-UMR 5183, 38402 Saint Martin d'Hère, France
[3]Université Savoie Mont-Blanc – LCME, 73376 Le Bourget du Lac CEDEX, France

Correspondence to: Lise Bonvalot (bonvalot@cerege.fr) and Edouard Bard (bard@cerege.fr)

Received: 24 April 2016 – Published in Atmos. Chem. Phys. Discuss.: 17 June 2016
Revised: 12 October 2016 – Accepted: 14 October 2016 – Published: 7 November 2016

Abstract. Atmospheric particulate matter (PM) affects the climate in various ways and has a negative impact on human health. In populated mountain valleys in Alpine regions, emissions from road traffic contribute to carbonaceous aerosols, but residential wood burning can be another source of PM during winter.

We determine the contribution of fossil and non-fossil carbon sources by measuring radiocarbon in aerosols using the recently installed AixMICADAS facility. The accelerator mass spectrometer is coupled to an elemental analyzer (EA) by means of a gas interface system directly connected to the gas ion source. This system provides rapid and accurate radiocarbon measurements for small samples (10–100 µgC) with minimal preparation from the aerosol filters. We show how the contamination induced by the EA protocol can be quantified and corrected for. Several standards and synthetic samples are then used to demonstrate the precision and accuracy of aerosol measurements over the full range of expected ^{14}C / ^{12}C ratios, ranging from modern carbon to fossil carbon depleted in ^{14}C.

Aerosols sampled in Chamonix and Passy (Arve River valley, French Alps) from November 2013 to August 2014 are analyzed for both radiocarbon (124 analyses in total) and levoglucosan, which is commonly used as a specific tracer for biomass burning. NO_x concentration, which is expected to be associated with traffic emissions, is also monitored.

Based on ^{14}C measurements, we can show that the relative fraction of non-fossil carbon is significantly higher in winter than in summer. In winter, non-fossil carbon represents about 85 % of total carbon, while in summer this proportion is still 75 % considering all samples. The largest total carbon and levoglucosan concentrations are observed for winter aerosols with values up to 50 and 8 µg m^{-3}, respectively. These levels are higher than those observed in many European cities, but are close to those for other polluted Alpine valleys.

The non-fossil carbon concentrations are strongly correlated with the levoglucosan concentrations in winter samples, suggesting that almost all of the non-fossil carbon originates from wood combustion used for heating during winter.

For summer samples, the joint use of ^{14}C and levoglucosan measurements leads to a new model to separately quantify the contributions of biomass burning and biogenic emissions in the non-fossil fraction. The comparison of the biogenic fraction with polyols (a proxy for primary soil biogenic emissions) and with the temperature suggests a major influence of the secondary biogenic aerosols.

Significant correlations are found between the NO_x concentration and the fossil carbon concentration for all seasons and sites, confirming the relation between road traffic emissions and fossil carbon.

Overall, this dual approach combining radiocarbon and levoglucosan analyses strengthens the conclusion concerning

the impact of biomass burning. Combining these geochemical data serves both to detect and quantify additional carbon sources. The Arve River valley provides the first illustration of aerosols of this model.

1 Introduction

Airborne particles, generally known as atmospheric aerosols or particulate matter (PM), are the focus of many environmental concerns. Indeed, airborne particles affect the climate on a regional (Penner et al., 1998; Chung and Seinfeld, 2002) and global (Ramanathan et al., 2001a, b) scale by modifying cloud properties (Jacobson et al., 2000) and by reflecting, scattering, and absorbing sunlight. Notably, the black carbon fraction of PM leads to the second largest anomaly of radiative forcing observed since the beginning of the industrial era, close behind anthropogenic CO_2 (Bond et al., 2013).

In addition, the harmful impact of PM on human health is well established: exposure to aerosols can cause respiratory and cardiopulmonary diseases that lead to increased mortality (Jerrett et al., 2005; Pope and Dockery, 2006; Kennedy, 2007; Lelieveld et al., 2015).

Carbonaceous particles constitute a major fraction (at least a third) of PM (Putaud et al., 2004, 2010). Their sources can be both biogenic and anthropogenic, leading to primary particles (i.e., directly emitted) and to secondary organic particles from gaseous precursors such as volatile organic compounds (Pöschl, 2005).

Improving the characterization of the relative contributions of anthropogenic and natural sources to PM is a crucial issue that has scientific and societal implications (Gustafsson et al., 2009). The importance of PM emission due to biomass burning (BB) for domestic heating has been shown for many urban areas (Jordan et al., 2006b; Zotter et al., 2014). The Arve River valley, located in the French Alps, is strongly impacted by pollution events and high PM concentrations. The severity of these events is due to a combination of topography and local meteorology, notably with temperature inversion layers during winter, which trap air masses close to the ground (Herich et al., 2014). Due to very limited exogenous contributions, notably during winter, the typology of aerosol sources remains simple, which constitutes an ideal site for testing a new method of aerosol source characterization.

The pollution of the Arve River valley has already been investigated using various techniques and results suggest the influence of local sources of carbon, more specifically from biomass burning used for residential heating during winter (Marchand et al., 2004; Aymoz et al., 2007; Herich et al., 2014). Different source apportionment models (Chemical Mass Balance, Positive Matrix Factorization, aethalometer) have been used to determine the contribution from biomass burning in a French Alpine city (Grenoble) (Favez et al., 2010), but significant discrepancies due to differences in the conceptual hypotheses made for each model are still observed.

Radiocarbon (^{14}C) measurement of the carbonaceous PM fraction has been demonstrated to be an effective tool for aerosol source apportionment, in particular for distinguishing fossil fuel combustion products from other carbon sources such as biomass burning and biogenic emissions (Jordan et al., 2006b; Szidat et al., 2006; El Haddad et al., 2011; Liu et al., 2013).

^{14}C is produced naturally in the upper atmosphere by the interaction of secondary neutrons from cosmic rays with nitrogen atoms. It is then oxidized into $^{14}CO_2$ and well mixed in the atmosphere before being partly taken up by vegetation during photosynthesis. Living organisms such as trees exhibit ^{14}C / ^{12}C ratios similar to that of the atmospheric pool on the order of 10^{-12}.

Biomass fuel is defined as a generic term meaning a source of modern carbon. Several factors cause the atmospheric ^{14}C / ^{12}C ratio to vary slightly from year to year, and this has been well documented over the last decades (Levin and Kromer, 2004; Hua et al., 2013; Levin et al., 2013). As a consequence, the ^{14}C / ^{12}C ratio in the biomass will also vary with the year of growth. By contrast, fossil fuels are depleted in ^{14}C as they are made of sedimentary organic matter, which is much older than the radioactive half-life of ^{14}C ($T_{1/2} = 5730$ years). Therefore, by measuring the ^{14}C in the whole carbonaceous fraction of aerosol samples, it is possible to quantify the fossil (f_F) and non-fossil (f_{NF}) fractions.

The direct coupling of an elemental analyzer (EA) to an accelerator mass spectrometer (AMS) is a fast and efficient way to measure the ^{14}C in small samples and, more particularly, in aerosols (Ruff et al., 2010a; Salazar et al., 2015). In our case, the CO_2 produced by combustion in the EA is delivered into the gas ion source of the AMS AixMICADAS (Bard et al., 2015) by means of the gas interface system (GIS) (Wacker et al., 2013). AixMICADAS is based on an updated version of the MICADAS (MIni CArbon DAting System) developed and constructed by ETH Zurich and now produced by the company IonPlus. In contrast to conventional offline solid AMS analyses where the sample preparation, i.e., graphitization, of very small samples (Genberg et al., 2010, 2013) is complex and time consuming, this method is now applied to very small samples (5–100 µgC) without complex preparation and handling problems. In the case of atmospheric PM samples, such a low required mass allows complementary analyses of other parameters on the same filter.

This study describes our protocol of PM sample analysis for ^{14}C, including the analyses of standards and blanks in order to quantify and correct for possible contamination (Ruff et al., 2010b). As an example of application, we then determine the fractions of fossil and non-fossil carbon in carbonaceous aerosols from the Arve River valley (French Alps), sampled in the cities of Passy and Chamonix, from November 2013 to August 2014. Levoglucosan, which is a biomass

burning molecular proxy (Simoneit et al., 1999), is measured in the same samples and is used to provide an independent view of the biomass burning contribution. NO_x levels are also monitored in parallel because they are mainly associated with traffic emissions. Polyols are measured as a proxy for primary biogenic aerosol particles.

2 Materials and methods

2.1 Radiocarbon measurements: method development

2.1.1 EA–GIS–AixMICADAS coupling

AixMICADAS is a compact AMS system dedicated to ^{14}C measurements in ultra-small samples (Synal et al., 2007; Bard et al., 2015). It operates at around 200 kV with carbon ion stripping in helium gas. It is equipped with a hybrid ion source that can handle both graphite targets and CO_2 gas (Fahrni et al., 2013; Wacker et al., 2013). It is coupled to a versatile gas interface system that ensures stable gas measurements from different sources: a cracker for CO_2 in glass ampoules, an automated system to handle carbonate, and an elemental analyzer for combusting organic matter. AixMICADAS and its performances are described elsewhere (Bard et al., 2015).

Atmospheric PM is collected on quartz filters, but only a small punch (between 0.2 and 1.5 cm^2, depending on the filter loading) is required for the ^{14}C analysis. The small filter punch is wrapped into a metallic boat before being combusted in the elemental analyzer. The sample preparation is carried out in a laminar flow hood to minimize contamination. The boats are made of silver ($10 \times 10 \times 20$ mm, about 240 mg each) and are baked at 800 °C for 2 h to eliminate organic contamination. The EA (vario Micro cube, Elementar) is equipped with a combustion tube filled with tungsten oxide granules (heated at 1050 °C) and a reduction tube filled with copper wires and silver wool (heated at 550 °C). The sample is oxidized in the combustion tube under an oxygen–helium atmosphere temporarily enriched with oxygen; the tungsten oxide bed supports the complete oxidation of combustion gases. Then, the evolved CO_2, water, and nitrogen oxides flow through the reduction tube (helium is used as carrier gas) where nitrogen oxides are reduced to N_2. A phosphorus pentoxide trap is then used to retain water produced during combustion and only the CO_2 is transferred and focused into the zeolite trap of the GIS. CO_2 is released by heating the trap to 450 °C and is then transferred into the injection syringe by gas expansion. The CO_2 is quantified before addition of helium to obtain a 5 % CO_2 mixture, which is finally injected into the ion source of AixMICADAS. An overall confidence interval of 4 % is considered for the carbon measurements. This conservative value is based on the average difference between several duplicate measurements of different aerosol samples. This 4 % value thus includes the intrinsic uncertainty of the measurement by the GIS, together with the additional uncertainty linked to loading heterogeneities at the surface of the filters and the difficulty in punching exactly the same surface of the filter. This 4 % uncertainty is propagated to all values related to the carbon mass.

Measured ^{14}C / ^{12}C ratios are corrected for fractionation based on the analysis of the ^{13}C ion beam on an AixMICADAS Faraday cup. ^{14}C data are then expressed as a normalized activity $F^{14}C$ ratio equivalent to fraction modern (Reimer et al., 2004).

Blank measurements are performed using CO_2 derived from fossil sources (without ^{14}C). Measurements of CO_2 produced from oxalic acid 2 standard (OxA2; National Institute of Standards and Technology, SRM 4990C) are used to normalize all ^{14}C / ^{12}C ratios of the measured samples. Both blank and standard CO_2 are contained in bottles directly coupled to the GIS and its injection syringe. During 2015, 85 blank gas samples were measured, giving an average $F^{14}C$ of 0.0045 (SD = 0.0019; $N = 85$; and $\sigma_{er} = 0.0002$, $\sigma_{er} = SD/N^{1/2}$). This result is equivalent to a radiocarbon age of $43\,400 \pm 360$ years. During the same year, we added 46 OxA2 gas samples, considered as unknown samples, which led to an average $F^{14}C$ of 1.3405 (SD = 0.0064, $N = 46$, and $\sigma_{er} = 0.0009$). These values are compatible with the standard value of 1.3407 ± 0.0005 $F^{14}C$ (Stuiver, 1983). OxA2 gas samples are considered as unknown samples so they are not used to correct and normalize measurements (i.e., machine transmission and chemistry fractionation) (Bard et al., 2015) and SD can be quantified.

In aerosol science, the fraction modern (f_M) is widely used. As underlined by Eriksson Stenström et al. (2011), it is not always clear if f_M has been corrected for decay since 1950 as in Currie et al. (1989). To avoid any confusion in our paper, all measurements will be expressed in $F^{14}C$ as defined by Reimer et al. (2004). $F^{14}C$ is defined as the ratio of the sample activity to the standard (OxA2) activity measured in the same year, with both activities background-corrected and $\delta^{13}C$-normalized (i.e., A_{SN}/A_{ON} with A_{SN} as the normalized specific activity of the sample and A_{ON} as the normalized specific activity of the OxA2). $F^{14}C$ does not depend on the year of measurement. Conversion between $F^{14}C$ and f_M (corrected for decay since 1950) is carried out following Eq. (1):

$$f_M = F^{14}C \times \exp\left[(1950 - T_m)/8267\right], \quad (1)$$

with T_m the year of measurement and 8267 corresponding to the true mean life of radiocarbon expressed in years, i.e., the true half-life 5730 years divided by ln(2). The exponential factor is slightly lower than one; thus, f_M is smaller than $F^{14}C$ (currently about 8 ‰). It is worth underlining that the non-fossil fraction f_{NF} and the fossil fraction f_F do not depend on the ^{14}C measurement unit. Indeed, f_{NF} and f_F are ratios between the sample measurement and a reference value, as detailed in Eq. (6), for the modern end-member (the fossil end-member staying at zero). As long as ^{14}C measure-

ments and end-members values are expressed in the same unit ($F^{14}C$ or f_M), f_{NF} and f_F do not vary with the year of measurement and values determined at different times can be compared.

2.1.2 Contamination quantification

It is initially assumed that a sample of a carbon mass M_S and a ^{14}C / ^{12}C ratio $F^{14}C_S$ analyzed with the EA-GIS coupling becomes contaminated with a constant mass of carbon M_C exhibiting a constant ^{14}C / ^{12}C ratio $F^{14}C_C$. The main source of contamination is likely to come from the silver boat: while the heat treatment can remove the carbon adsorbed on metallic surfaces of the boat, carbon impurities occluded in the silver cannot be removed. By using the EA, we previously quantified the carbon content of empty silver boats, resulting in a contamination on the order of 1–2 µgC per boat. Similar carbon contaminations have been quantified by Ruff et al. (2010b) for smaller tin boats. Other sources of carbon may potentially originate in the preparation of the sample (filter) or even from EA-GIS coupling.

The ultimate contamination of metallic boats will be considered as constant. This assumption is expressed in the following mass balance Eqs. (2) and (3) where M_M and $F^{14}C_M$ represent the measured mass and the measured isotopic ratio, respectively (Ruff et al., 2010a):

$$F^{14}C_M \times M_M = F^{14}C_S \times M_S + F^{14}C_C \times M_C \quad (2)$$

$$M_M = M_S + M_C. \quad (3)$$

In order to determine M_C and $F^{14}C_C$ and to test the assumption of constant values, blank and standard samples were measured with various masses M_M. Phthalic acid (PA) blank ($F^{14}C = 0$) and OxA2 standard were diluted in ultrapure water and various volumes (less than 25 µL) were deposited onto a quartz filter (Pall Flex QAT) punch of approximately 1 cm^2 which had been pre-baked at 500 °C for 2 h. Spiked filter punches were wrapped in silver boats and then loaded into the EA autosampler.

Combining Eqs. (2) and (3) leads to Eq. (4) in which the measured values M_M and $F^{14}C_M$ and the known $F^{14}C_S$ values are used to derive M_C and $F^{14}C_C$ of the contaminating carbon.

$$F^{14}C_M = \frac{(M_M - M_C) \times F^{14}C_S + M_C \times F^{14}C_C}{M_M} \quad (4)$$

OxA2 and PA samples with different carbon mass (M_M) were measured and a nonlinear weighted least squares method (weights corresponding to the measured uncertainties on $F^{14}C_M$ values) was applied to determine $F^{14}C_C$ and M_C. The results of the contamination model for the blank and the standard are represented in Fig. 1a; the estimated parameters from the fit are $F^{14}C_C = 0.73 \pm 0.11$ and $M_C = 1.45 \pm 0.26$ µgC (95 % confidence interval). Figure 1b and c depicts the same dataset corrected for the contamination parameters. It can be observed that $F^{14}C_S$ values for PA and OxA2 are in agreement with the expected values, confirming the constant contamination assumption. Contamination studies were also carried out without filter punches (the blank and standard are laid in solid forms in the silver boats), leading to similar contamination parameters. It may thus be deduced that the boats are the primary source of contamination.

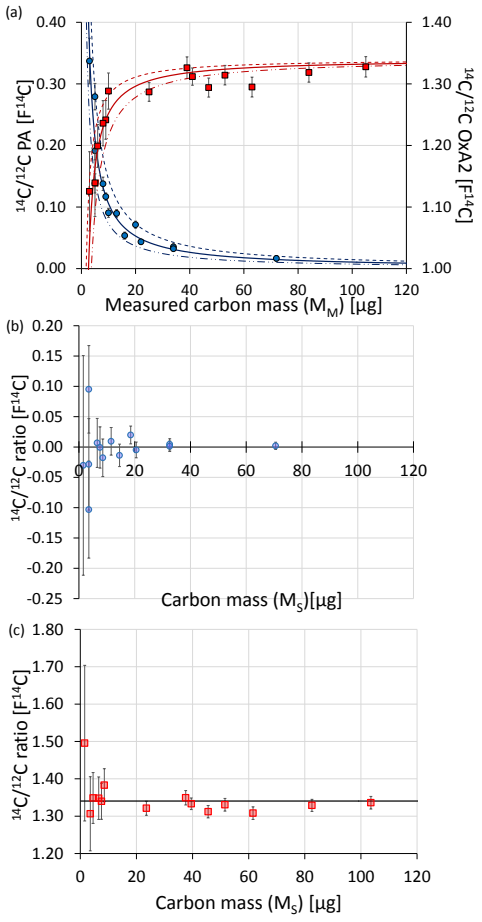

Figure 1. Measurements and corrections for blank (phthalic acid, PA) and standard (oxalic acid 2, OxA2) samples. **(a)** Blue dots represent the measured ^{14}C / ^{12}C ratio for sample blanks and red squares stand for standard measurements. Solid lines and dashed lines represent the least square optimization with its 95 % confidence interval. M_M is the measured carbon mass. **(b)** Blue dots are the corrected blank measurements. M_S is the sample carbon mass (i.e., the measured carbon mass corrected for the contaminant carbon mass). **(c)** Red squares are the corrected standard measurements and the line at 1.3406 stands for the certified value of OxA2. M_S is the sample carbon mass (i.e., the measured carbon mass corrected for the contaminant carbon mass). The results shown in **(b)** (blank) and **(c)** (standard) illustrate the quality of the correction.

2.1.3 Standard and synthetic aerosol samples

In order to mimic aerosol samples, two NIST standards were used as end-members and were mixed together to simulate different ^{14}C / ^{12}C ratios: SRM (Standard Reference Material) 2975 Forklift Diesel Soot (78 % carbon) and SRM 1515 Apple Leaves (45 % carbon). The first standard typifies fossil fuel combustion products while the second provides an analog of natural biopolymers generally found in PM (Currie and Kessler, 2005). ^{14}C / ^{12}C ratios were determined by performing precise measurements on large samples, of roughly 1 mgC, that were graphitized with the AGE-3 system (Automated Graphitization Equipment, described in Wacker et al., 2010) and analyzed with AixMICADAS using its hybrid ion source in the conventional mode. As expected, SRM 2975 exhibits a very low ^{14}C / ^{12}C ratio ($F^{14}C = 0.0013$ with SD = 0.0002, $N = 5$, and $\sigma_{er} = 0.0001$, blank subtracted) whereas SRM 1515 has the ^{14}C / ^{12}C ratio of the atmosphere at the time of its photosynthesis in 1985 ($F^{14}C = 1.1862$ with SD = 0.0017, $N = 5$, and $\sigma_{er} = 0.0007$).

Mixtures of the two SRM standards were prepared to obtain different ^{14}C / ^{12}C ratios. To ensure homogeneity, the standards were mixed with an agate mortar and pestle. The relative proportion of modern carbon can be defined as follows in Eq. (5):

$$X_{\text{modern carbon}} = \frac{mC_{SRM1515}}{mC_{SRM1515} + mC_{SRM2975}} = \frac{0.45 \times m_{SRM1515}}{0.45 \times m_{SRM1515} + 0.78 \times m_{SRM2975}}. \quad (5)$$

Expected $F^{14}C$ values were calculated by using the mass of each SRM and their measured $F^{14}C$ as end-members. The uncertainties were calculated by propagating different sources of errors: the weighing uncertainty on the mass of each standard and the analytical uncertainties of the ^{14}C / ^{12}C ratio of the pure standards. All mixed samples were graphitized with the AGE-3 system and measured with AixMICADAS (three measurements for each mixture). The small scatter of the results listed in Table 1 confirms that mixtures were well homogenized and that ^{14}C / ^{12}C ratio determinations are reproducible. In addition, the good agreement between theoretical and measured values confirms that these mixtures can be used to simulate small aerosol samples.

Following this initial step, the SRM mixtures were loaded onto quartz filters. In order to simulate real aerosol samples, each powder mixture was suspended in ultrapure water. Different volumes of these suspensions (about 80 µgC mL^{-1}) were then deposited onto quartz filters that had been baked previously at 500 °C for 2 h. A vacuum filtration system (Millipore) was used to eliminate most of the water and to distribute carbonaceous particles evenly over the filter surface. Loaded filters were dried overnight in a laminar airflow hood and then subsampled with a puncher ($d = 11$ mm, $S = 0.95$ cm^2) before being loaded into silver boats. Each

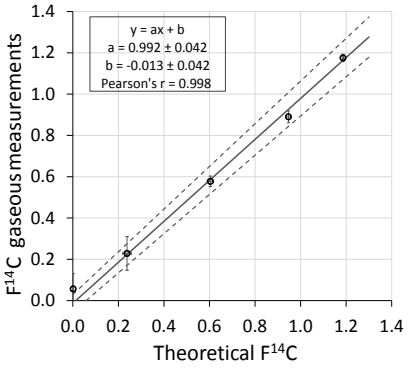

Figure 2. $F^{14}C$ values of synthetic and standard (test) aerosol samples measured with the gas source compared with theoretical values. These test aerosols are made of two Standard Reference Materials (SRM 2975 and SRM 1515). The compositions of the different mixtures are listed in Table 1 with the corresponding theoretical and measured $F^{14}C$. The coefficients of the linear regression have been calculated by taking into account error bars (2 SD) on both axes and are given with their 95 % confidence interval. The linear relation confirms the accuracy of aerosol measurements with the gas ion source over the full range of expected ^{14}C activities.

standard mixture was measured at least four times with different carbon masses, corresponding to different loadings on independent filters. Mean results shown in Fig. 2 confirm the accuracy of aerosol measurements with the gas ion source over the full range of expected ^{14}C activities ($F^{14}C$ between 0.001 and 1.2).

To further test the precision and accuracy of the developed aerosol analytical procedures, we also analyzed two standards prepared from atmospheric particle matter (Table 2).

We acquired NIST SRM 1649b, prepared from the same bulk material as the original SRM 1649 and SRM 1649a (which are no longer available) but sieved to a smaller particle size fraction (63 µm). The original bulk material, SRM 1649 was prepared at NIST from PM collected in 1976–1977 in the Washington, DC, area over a 12-month period and issued in 1982 (Wise and Watters, 2007, 2009).

High-precision measurements were performed to determine the ^{14}C / ^{12}C ratio of NIST SRM 1649b. Samples were converted to graphite with the AGE-3 system. Four solid targets (≈ 1 mgC) were measured. Online gas measurements were also investigated using quartz filters loaded with NIST SRM 1649b. In short, SRM 1649b was suspended in ultrapure water (about 80 µgC mL^{-1}) and deposited onto previously baked quartz filters. Loaded filters were then dried in the clean hood, punched, and wrapped into silver boats, ready for use with the EA-GIS coupled to AixMICADAS. The replicates ($N = 7$) were obtained with carbon mass ranging from 7 to 93 µgC.

Our graphite measurements of large samples are in agreement with the values reported in the literature for SRM 1649 and SRM 1649a (Currie et al., 1984, 2002; Szidat et al., 2004;

Table 1. Analyses of mixtures of SRM 2975 and SRM 1515 standards in the form of solid graphite targets of large samples (roughly 1 mgC). X modern carbon represents the mass fraction of modern carbon; see Eq. (5). The mass fraction of each SRM can be calculated using their carbon content (i.e., 45 % for SRM1 515 and 78 % for SRM 2975). "Expected F^{14}C" is calculated by using the mass of each SRM and its measured F^{14}C as end-members. Measurements are made with solid target (graphitization, roughly 1 mgC).

X modern carbon	Expected F^{14}C	Standard error [F^{14}C]	Measured F^{14}C (after graphitization)	Standard deviation [F^{14}C]
0	0.0013	0.0001	0.0013	0.0002 ($N = 5$)
0.2	0.2379	0.0185	0.2297	0.0002 ($N = 3$)
0.51	0.6039	0.0131	0.5896	0.0003 ($N = 5$)
0.8	0.9467	0.0096	0.9411	0.0012 ($N = 3$)
1	1.1862	0.0007	1.1862	0.0017 ($N = 5$)

Table 2. Analyses of SRM1949b with gaseous and solid (roughly 1 mgC) source. Gaseous measurements are made with punches of loaded quartz filters. Comparison with the literature values for SRM 1649 and SRM 1649a.

Gaseous source F^{14}C	SD ($N = 7$)	Solid source F^{14}C	SD ($N = 4$)	Literature values F^{14}C
0.505	0.028	0.532	0.004	Solid measurement SRM 1649a: 0.523 ± 0.018 ($N = 5$) (Szidat et al., 2004) 0.507–0.61, depending on the sample preparation (Currie et al., 2002; Wise and Watters, 2007) 0.517/0.572 (simple/double combustion) (Heal et al., 2011) Solid measurement SRM 1649: 0.61 ± 0.04 (Currie et al., 1984)

Wise and Watters, 2007; Heal et al., 2011). The F^{14}C value for the online gas measurements is 0.505, with a SD of 0.028, $N = 7$, and a σ_{er} of 0.010, whereas the determined F^{14}C for the solid measurements is 0.532 with a SD of 0.004, $N = 4$, and a σ_{er} of 0.002.

Two suggestions could be proposed to explain the small difference between solid and gaseous measurements. Some colloidal fraction or some water-soluble compounds may have been lost during sample preparation. If the soluble and insoluble fractions are of different origins, associated with different isotopic compositions, this could bias the $^{14}C / ^{12}C$ ratio of the residual material loaded on the filter. Similarly, the ultrafine fraction (< 0.3 µm) not retained by the filter may have a different isotopic carbon composition, leading to the discrepancy between the solid and gaseous measurements.

Such a problem does not affect our results on mixtures of SRM 2975 and SRM 1515 standards described previously; indeed, these standards are more prone to be isotopically homogeneous because of their simpler composition, as they both originate from one source.

The second reference material is RM 8785, composed of the fraction lower than 2.5 µm (i.e., $PM_{2.5}$) of SRM 1649 which has been resuspended in air and deposited onto quartz filters by NIST and SRI International (Cavanagh and Watters, 2005; Klouda et al., 2005). Analyses of three punches give an average F^{14}C of 0.387 and SD of 0.008. This value is in agreement which measurements performed by five different laboratories (Szidat et al., 2013), even if it is positioned at the high end of the values (Fig. 3). Szidat et al. (2013) pointed out that $^{14}C / ^{12}C$ results for RM 8785 exhibit a larger scatter than that measured on other PM samples during the same intercomparison of laboratories. This was probably caused by heterogeneous loading during production of RM 8785 filters by NIST (concentrations ranging from 92 to 2855 µg on to 8.55 cm^2 (Cavanagh and Watters, 2005)) or by secondary deposition of volatile organic compounds (VOCs) onto the filters.

An additional source of $^{14}C / ^{12}C$ scatter may be linked to the heterogeneity of fine particles (< 2.5 µm) constituting RM 8785. Indeed, its average F^{14}C value of approximately 0.39 is quite different from the value of approximately 0.5 measured for SRM 1649a, which was sieved at 125 µm only, and which is the raw material used to produce RM 8785. This suggests the possibility of isotopic heterogeneities between different particle sizes.

2.2 Samples from the Arve River valley

2.2.1 Sampling sites and procedures

The measurements were performed in the framework of the DECOMBIO (deconvolution combustion biomass) program (Chevrier et al., 2016), which focuses on the source appor-

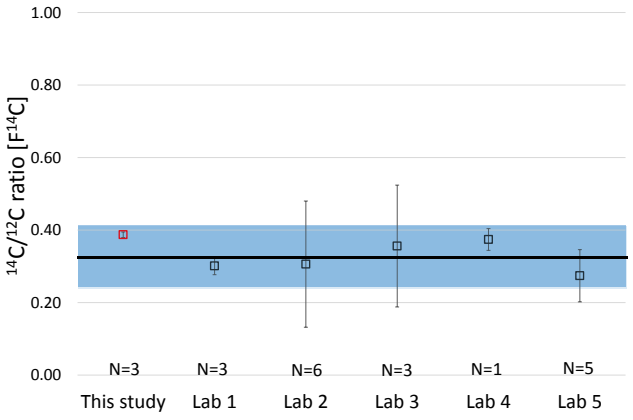

Figure 3. RM 8785 measurements. Black squares and error bars represent values and measurement uncertainties at 2σ, described in Szidat et al. (2013). The black line stands for the average value and the blue ribbon represents the 2σ confidence interval for Labs 1–5. The red square shows the weighted average result obtained for this study ($N = 3$) and its weighted error (2σ). The large scatter could be linked to heterogeneous loading during the production of RM 8785 as mentioned by Cavanagh and Watters (2005). The value obtained in this study is compatible with the high end of measurements performed by the five different laboratories.

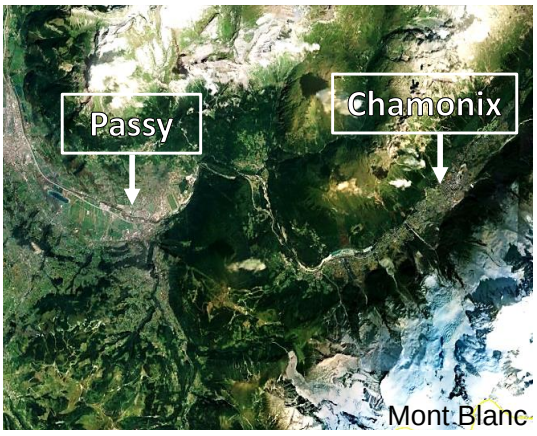

Figure 4. Location of the sampling stations in the Arve River valley investigated in this study. PM was sampled between November 2013 and August 2014 in Passy and between December 2013 and January 2014 in Chamonix. Both are urban stations, collecting the PM_{10} fraction of atmospheric aerosols.

tionment of PM_{10} in the Arve River valley and the evolution of the contribution of biomass burning emissions. Filters analyzed in our study were collected between November 2013 and August 2014 in Passy and between December 2013 and January 2014 in Chamonix. Both urban stations, maintained by the local Air Monitoring Agency (Air Rhône-Alpes) are located in the Arve River valley, in the French Alps. The collection sites are presented in Fig. 4. Sampling in the city of Passy (12 000 inhabitants) was performed at 583 m a.s.l. (above sea level) whereas sampling in Chamonix (9000 inhabitants) took place at 1035 m a.s.l. For both sampling sites the PM collection occurs about 4 m above the ground. The Passy sampling station is located in a parking lot, 20 m from the closest house and 90 m from a road. The Chamonix sampling occurred in the city center, close to shops. Temperatures were monitored hourly at both sites throughout the sampling period. Daily PM_{10} samples were collected on a quartz filter, using a Digitel DA-80 High Volume Sampler (30 $m^3\,h^{-1}$). All filters (quartz filters, Pall Tissu Quartz, 150 mm Ø) were pre-baked at 500 °C for 8 h. They were stored in aluminum foil and sealed in a polyethylene sheath before the PM sampling. After collection, filters were folded, wrapped in aluminum foils, sealed in polyethylene bags, and stored at −20 °C.

2.2.2 Additional data

Levoglucosan (1,6-anhydro-b-D-glucopyranose) is an anhydro-sugar, emitted by the pyrolysis of cellulose (Simoneit et al., 1999) and is widely used as a biomass burning tracer (Schauer et al., 2001; Jordan et al., 2006a; Caseiro et al., 2009). Here, the levoglucosan is water extracted and then quantified by high-performance liquid chromatography coupled with pulsed amperometric detection (Dionex, HPLC DX500 and PAD ED40) (Waked et al., 2014). The concentrations of several polyols (arabitol, mannitol, sorbitol) are also determined by this analysis. Polyols at high concentration in the atmospheric PM are known to originate from emission from fungi from soils (Yttri et al., 2007; Bauer et al., 2008).

TC (total carbon) concentration is also quantified on the same filters as the determination of the EC (elemental carbon) and OC (organic carbon) by thermal-optical analysis (TOA) EUSAAR2 (Cavalli et al., 2010) with a Sunset apparatus (Birch and Cary, 1996). TC is equal to the sum of EC and OC. PM_{10} total mass is measured online by TEOMS-FDMS (TEOM 1400ab and FDMS 8500c from Thermo Scientific), taking into account the volatile and nonvolatile fractions of the PM. NO_x ($NO + NO_2$) are also measured online (with the Environnement S.A. AC32M nitrogen oxides analyzer) and are used as proxies for traffic emissions.

2.2.3 Radiocarbon analyses

All samples were analyzed twice to increase the precision of ^{14}C / ^{12}C and carbon mass data and to check for possible heterogeneity of individual filters. This represents a total of 124 measurements including the sampling blanks (4 field blanks for Chamonix and 12 for Passy). Blank sampling filters are treated as real samples (in the lab and in the field) with the exception that no actual sampling is carried out: they are used to ensure that no significant contamination occurs during the different steps of the sampling campaign (e.g., during storage or transport).

Table 3. Results of analysis of Passy samples. PM_{10} is determined by TEOM-FDMS; days with a PM_{10} concentration higher than 50 µg m^{-3} (winter smog) are reported in bold italics (19 February 2014 is sampled with two filters and the sum is greater than 50 µg m^{-3}). Levoglucosan and NO_x concentrations: see text. Carbon concentration is determined using the GIS quantification and is expressed with its confidence interval. Each radiocarbon value (expressed in $F^{14}C$ and f_M) is based on duplicate measurements: here the weighted mean and its weighted error (2σ, i.e., 95 % confidence interval) are presented. For winter, it is considered that all the non-fossil carbon originates from biomass burning (i.e., $f_{NF,ref} = F^{14}C_{bb}$), whereas all the non-fossil carbon during summer is assumed to originate from biogenic emissions (i.e., $f_{NF,ref} = F^{14}C_{bio}$). The reference values ($f_{NF,ref}$) for winter and summer are expressed in $F^{14}C$ and f_M. Fossil and non-fossil fractions (f_F and f_{NF}) are determined by the radiocarbon measurements (see Eq. 6).

Date dd/mm/yyyy	PM_{10} [µg m^{-3}]	Carbon mass [µgC m^{-3}]	±Carbon mass [µgC m^{-3}]	Levoglucosan [µg m^{-3}]	NO_x [µg m^{-3}]	$F^{14}C$	$\pm F^{14}C$	f_M	$\pm f_M$	f_{NF}	f_F	$\pm f_F/f_{NF}$
Winter $f_{NF,ref} = 1.10F^{14}C = 1.09\ f_M$												
24/11/2013	31	15.95	0.46	2.37	Nd	0.986	0.010	0.978	0.010	0.90	0.10	0.02
03/12/2013	***90***	***48.29***	***1.39***	***6.94***	***Nd***	***1.002***	***0.010***	***0.994***	***0.010***	***0.91***	***0.09***	***0.02***
05/12/2013	***60***	***24.56***	***0.73***	***3.50***	***Nd***	***0.977***	***0.011***	***0.970***	***0.011***	***0.89***	***0.11***	***0.02***
06/12/2013	***69***	***37.69***	***1.10***	***5.14***	***Nd***	***1.015***	***0.011***	***1.007***	***0.010***	***0.92***	***0.08***	***0.02***
08/12/2013	***75***	***38.58***	***1.12***	***6.03***	***Nd***	***1.047***	***0.011***	***1.039***	***0.011***	***0.95***	***0.05***	***0.02***
09/12/2013	***93***	***45.87***	***1.33***	***6.26***	***Nd***	***0.969***	***0.010***	***0.962***	***0.010***	***0.88***	***0.12***	***0.02***
12/12/2013	***133***	***53.81***	***1.55***	***7.66***	***177***	***0.987***	***0.010***	***0.979***	***0.010***	***0.90***	***0.10***	***0.02***
13/12/2013	***133***	***57.14***	***1.65***	***8.48***	***170***	***0.985***	***0.010***	***0.977***	***0.010***	***0.90***	***0.10***	***0.02***
15/12/2013	***86***	***34.46***	***1.01***	***5.81***	***68***	***1.067***	***0.011***	***1.059***	***0.011***	***0.97***	***0.03***	***0.02***
16/12/2013	***108***	***42.04***	***1.22***	***6.29***	***145***	***0.964***	***0.010***	***0.956***	***0.010***	***0.88***	***0.12***	***0.02***
18/12/2013	***82***	***28.78***	***0.85***	***4.60***	***120***	***0.926***	***0.010***	***0.919***	***0.010***	***0.84***	***0.16***	***0.02***
20/12/2013	***60***	***25.20***	***0.74***	***4.20***	***81***	***1.003***	***0.011***	***0.995***	***0.010***	***0.91***	***0.09***	***0.02***
01/01/2014	25	7.81	0.23	1.15	25	0.978	0.011	0.971	0.010	0.89	0.11	0.02
22/01/2014	41	17.35	0.50	2.63	57	0.957	0.011	0.949	0.010	0.87	0.13	0.02
12/02/2014	21	7.80	0.23	0.97	34	0.924	0.010	0.917	0.010	0.84	0.16	0.02
13/02/2014	18	6.45	0.20	0.83	23	0.980	0.012	0.972	0.011	0.89	0.11	0.02
15/02/2014	13	3.76	0.12	0.47	13	0.875	0.013	0.868	0.013	0.80	0.20	0.02
16/02/2014	43	16.48	0.48	2.61	32	1.026	0.011	1.018	0.011	0.93	0.07	0.02
19/02/2014	***38***	***17.06***	***0.49***	***2.69***	***Nd***	***0.976***	***0.011***	***0.968***	***0.011***	***0.89***	***0.11***	***0.02***
19/02/2014	***37***	***17.39***	***0.50***	***2.65***	***Nd***	***0.924***	***0.011***	***0.917***	***0.011***	***0.84***	***0.16***	***0.02***
21/02/2014	29	12.06	0.35	1.71	35	1.046	0.011	1.038	0.011	0.95	0.05	0.02
22/02/2014	22	7.08	0.21	0.93	24	1.011	0.011	1.003	0.011	0.92	0.08	0.02
24/02/2014	38	16.17	0.39	2.09	46	0.878	0.008	0.871	0.008	0.80	0.20	0.02
25/02/2014	37	9.81	0.29	1.30	40	0.921	0.011	0.914	0.011	0.84	0.16	0.02
27/02/2014	33	12.37	0.36	1.66	46	0.956	0.011	0.949	0.011	0.87	0.13	0.02
28/02/2014	20	8.81	0.26	1.31	21	1.004	0.011	0.996	0.011	0.91	0.09	0.02
02/03/2014	20	7.25	0.22	1.12	15	1.033	0.011	1.025	0.011	0.94	0.06	0.02
Summer $f_{NF,ref} = 1.04\ F^{14}C = 1.03\ f_M$												
28/07/2014	15	3.45	0.11	0.03	14	0.714	0.012	0.708	0.012	0.69	0.31	0.01
30/07/2014	12	2.81	0.10	0.03	17	0.625	0.015	0.620	0.014	0.60	0.40	0.02
31/07/2014	13	3.33	0.11	0.03	11	0.686	0.013	0.680	0.013	0.66	0.34	0.01
02/08/2014	17	3.13	0.11	0.03	10	0.815	0.014	0.809	0.014	0.78	0.22	0.02
03/08/2014	13	2.81	0.10	0.04	6	0.879	0.016	0.872	0.016	0.85	0.15	0.02
05/08/2014	16	3.66	0.12	0.03	11	0.815	0.013	0.809	0.013	0.78	0.22	0.01
06/08/2014	21	4.74	0.15	0.04	15	0.771	0.011	0.765	0.011	0.74	0.26	0.01
08/08/2014	10	3.17	0.11	0.02	14	0.717	0.013	0.711	0.013	0.69	0.31	0.01
09/08/2014	11	3.12	0.10	0.06	11	0.823	0.014	0.816	0.014	0.79	0.21	0.02
11/08/2014	13	2.50	0.09	0.06	13	0.771	0.017	0.764	0.017	0.74	0.26	0.02
12/08/2014	13	2.73	0.10	0.05	10	0.829	0.016	0.822	0.016	0.80	0.20	0.02
14/08/2014	8	1.97	0.08	0.04	9	0.794	0.021	0.788	0.020	0.76	0.24	0.02
15/08/2014	7	2.32	0.09	0.13	9	0.890	0.020	0.883	0.020	0.86	0.14	0.02
17/08/2014	9	2.39	0.09	0.04	7	0.824	0.018	0.817	0.018	0.79	0.21	0.02

Table 4. Results of analysis of Chamonix samples. PM_{10} is determined by TEOM-FDMS; days with a PM_{10} concentration higher than $50\,\mu g\,m^{-3}$ (winter smog) are reported in bold italic. Levoglucosan and NO_x concentrations: see text. Carbon concentration is determined using the GIS quantification and is expressed with its confidence interval. Each radiocarbon value (expressed in $F^{14}C$ and f_M) is based on duplicate measurements: here the weighted mean and its weighted error (2σ i.e., 95 % confidence interval) are presented. Fossil and non-fossil fractions (f_F and f_{NF}) are determined by the radiocarbon measurements (see Eq. 6).

Date dd/mm/yyyy	PM_{10} [$\mu g\,m^{-3}$]	Carbon mass [$\mu gC\,m^{-3}$]	±Carbon mass [$\mu gC\,m^{-3}$]	Levoglucosan [$\mu g\,m^{-3}$]	NO_x [$\mu g\,m^{-3}$]	$F^{14}C$	$\pm F^{14}C$	f_M	$\pm f_M$	f_{NF}	f_F	$\pm f_F/f_{NF}$
05/12/2013	44	19.75	0.57	2.66	174	0.900	0.011	0.893	0.011	0.82	0.18	0.02
08/12/2013	44	24.80	0.73	3.83	129	1.017	0.012	1.009	0.012	0.92	0.08	0.02
11/12/2013	***63***	***29.52***	***0.87***	***3.87***	***250***	***0.872***	***0.010***	***0.865***	***0.010***	***0.79***	***0.21***	***0.02***
14/12/2013	40	20.97	0.60	3.23	133	0.968	0.011	0.961	0.011	0.88	0.12	0.02
17/12/2013	***53***	***29.97***	***0.88***	***3.45***	***263***	***0.865***	***0.011***	***0.858***	***0.011***	***0.79***	***0.21***	***0.02***
20/12/2013	18	7.08	0.21	0.87	74	0.841	0.011	0.834	0.011	0.76	0.24	0.02
23/12/2013	39	20.09	0.60	3.02	170	0.914	0.011	0.907	0.011	0.83	0.17	0.02
26/12/2013	14	5.73	0.18	0.79	57	0.918	0.012	0.911	0.011	0.83	0.17	0.02
29/12/2013	18	8.36	0.25	1.17	67	0.943	0.013	0.935	0.013	0.86	0.14	0.02
01/01/2014	***61***	***26.29***	***0.77***	***4.21***	***154***	***1.018***	***0.012***	***1.010***	***0.012***	***0.93***	***0.07***	***0.02***
04/01/2014	17	8.48	0.25	1.23	82	0.942	0.011	0.934	0.011	0.86	0.14	0.02
07/01/2014	36	19.83	0.57	2.86	161	0.897	0.011	0.890	0.011	0.82	0.18	0.02

Punch surface required for radiocarbon analysis (i.e., punch of 1 or 0.4 cm^2, depending on the carbon loading of the filter) was determined using the total carbon concentration previously determined by the EC / OC thermal-optical analysis at LGGE (Grenoble). In this study, the carbon quantity is also determined by the GIS before CO_2 injection into the ion source.

The mean carbon mass of the sampling blank filters determined by the GIS system is 1.75 µgC (SD = 1.22 µgC, $N = 16$). This contamination level agrees with the independent blank assessment described in Sect. 2.1.2. For real aerosol samples, the carbon mass and ^{14}C / ^{12}C ratios are thus corrected in the same way as described previously.

The carbon content data measured by TOA in the LGGE (Grenoble) and by the GIS in the CEREGE (Aix-en-Provence) are compared in Fig. 5, exhibiting a very strong linear correlation for both sites (treated together). The slope is close to 1, with a very small intercept, suggesting there is no major difference between measurements obtained on different punch subsamples. This also demonstrates that sampling filters are loaded relatively homogenously.

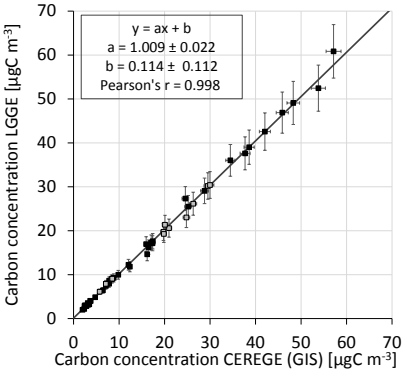

Figure 5. Total carbon concentration measurements. Comparison between TOA (LGGE in Grenoble) and GIS (CEREGE in Aix-en-Provence) measurements. The grey squares stand for the Chamonix samples and the black squares stand for the Passy samples. The regression parameters, given with their 95 % confidence intervals, have been calculated by taking into account error bars on both axes and exhibit a very good correlation between the two carbon concentrations; the two sets of measurements can be considered as equivalent.

3 Results and discussion

3.1 Composition of PM_{10}

For both sites, summer samples exhibit daily average PM_{10} concentrations up to 21 $\mu g\,m^{-3}$ while winter PM_{10} concentrations range from 13 to 133 $\mu g\,m^{-3}$. Above the public information threshold, 12 days in Passy and 3 days in Chamonix exceed $50\,\mu g\,m^{-3}$ and correspond to winter smog episodes (see Tables 3 and 4). On average, winter samples are composed of about 45 % carbon (for both Passy and Chamonix), while summer samples in Passy comprise 25 % carbon only. The carbon concentration in Passy is very high during the winter season (average of 23 $\mu gC\,m^{-3}$), particularly during December with a mean concentration of 40 $\mu gC\,m^{-3}$. It is much lower during July and August at about 3 $\mu gC\,m^{-3}$. The mean carbon concentration in Chamonix for December and January is about 18 $\mu gC\,m^{-3}$. Therefore, the December average carbon load in Passy is about twice that in Chamonix. Passy is a populated area, located in the lower part of the Arve River valley, with a valley constriction (steep slopes and reduced sun exposure) limiting atmospheric mixing in win-

ter. High emissions and a strong temperature inversion layer persisting for several consecutive days lead to very high particle concentrations when compared to those in Chamonix.

These winter carbon concentrations are an order of magnitude higher than those determined in Gothenburg (Sweden) during February and March 2005 ($3\,\mu gC\,m^{-3}$) (Szidat et al., 2009) or in Hachioji (Japan) during the 2003 and 2004 winter seasons (less than $3\,\mu gC\,m^{-3}$) (Uchida et al., 2010). Comparable concentrations were observed in Switzerland (Szidat et al., 2007) in Roveredo (about $16\,\mu gC\,m^{-3}$, January 2005) and Moleno (about $24\,\mu gC\,m^{-3}$, February 2005), places that are also typical Alpine valley sites similar to Passy and Chamonix.

The summer mean level of levoglucosan in Passy is close to $0.03\,\mu g\,m^{-3}$, which is comparable to summer background concentrations determined by Puxbaum et al. (2007) for six background stations located on an east–west line from Hungary to the Azores. At our sites, winter levels are about 100 times greater than summer ones: in Chamonix, the average concentration is about $2.6\,\mu g\,m^{-3}$, while in Passy it is about $3.4\,\mu g\,m^{-3}$ (up to $8.5\,\mu g\,m^{-3}$). These levels are similar to those found in Launceston (Australia) during winter 2003 (Jordan et al., 2006a) but are generally higher than winter levels measured in various European cities (Herich et al., 2014).

Recent studies report that levoglucosan can be partially degraded by photo-oxidation (Hennigan et al., 2010; Kessler et al., 2010) for summer conditions, suggesting that this proxy is not as stable as previously thought. However, as winter temperatures are low (on average between 0 and $-2.5\,°C$) and photo-oxidation is reduced by meteorological conditions (reduced daylight period, strong presence of smog and clouds) during this season, the levoglucosan level is expected to be particularly stable during winter. In addition, in our study sampling was carried out close to the emission sources, limiting the exposure time and thus any possible degradation, even during summer.

Levoglucosan emission rate depends on various factors, such as the combustion type and conditions (Engling et al., 2006; Schmidl et al., 2008; Lee et al., 2010). Wood type (softwoods and hardwoods) also has an influence on the emission factor of levoglucosan: as ambient measurements generally represent a mixture of different fuels and combustion conditions, the relation between levoglucosan and PM emissions can vary.

3.2 ^{14}C-based source apportionment

Carbon in atmospheric aerosols can originate from both fossil and contemporary sources. Carbon in particles from fossil fuel emissions is characterized by $F^{14}C = 0$, due to the radioactive decay (half-life of 5730 years), whereas $F^{14}C \approx 1$ for carbon in particles coming from contemporary sources. In addition, the atmospheric thermonuclear bomb tests of the late 1950s and early 1960s increased the ^{14}C content of the atmosphere, leading to $F^{14}C$ contemporary values greater than 1. In the Northern Hemisphere, the bomb spike reached $F^{14}C$ values on the order of 1.8 in the early 1960s and has decayed asymptotically since that time (Levin et al., 2010, 2013; Hua et al., 2013). From these studies, the atmospheric value for the year 2013–2014 can be estimated at $F^{14}C_{atmo} = 1.04$. Hence, biogenic emissions from these years will present the same value ($F^{14}C_{bio} = 1.04$).

3.2.1 Apportionment of the carbon pool with a simple hypothesis

In a first and preliminary approximation, we assume that the carbonaceous fraction is composed of both a fossil fraction, without ^{14}C and so linked to fossil fuels, and an isotopically homogenous non-fossil fraction. To determine this non-fossil fraction (f_{NF}), the measured $F^{14}C$ has to be normalized by a non-fossil reference value ($f_{NF,ref}$, expressed in $F^{14}C$) as described by Eq. (6).

$$f_{NF} = \frac{F^{14}C}{f_{NF,ref}} \quad (6)$$

The high levels of levoglucosan obtained during winter illustrate the significance of biomass burning at both sites during the cold season while summer values suggest that very little biomass burning is recorded for the warm season. Biomass burning is mainly based on wood that grew over the past decades. This means that this carbon fraction integrates an average $F^{14}C$ that is slightly higher than that of the atmosphere at the time of sampling. As per Szidat et al. (2006) and Lewis et al. (2004), we assume that wood used for biomass burning has an average $F^{14}C_{bb} = 1.10$ ($f_{M,bb} = 1.09$), which can be retrieved from the atmospheric ^{14}C record combined with a tree growth model.

For the summer season, it is considered that all non-fossil carbon originates from organic compounds naturally released by living plants (Guenther et al., 1995). No wildfire was recorded during the sampling period and the influence of the charcoal from barbecue cooking is neglected; levels of cholesterol, generally emitted by meat charbroiling (Schauer et al., 1999) remain very low, indicating that this cooking technique is not important here. Therefore, only the biogenic source of aerosols is considered, whose $F^{14}C$ value should be close to the atmospheric value at the time of sampling ($F^{14}C_{bio} = 1.04$).

Hence, for this first estimation of the non-fossil and fossil fractions, $f_{NF,ref}$ is estimated to be equal to 1.10 $F^{14}C$ for the winter samples and to 1.04 $F^{14}C$ for the summer ones.

The calculated non-fossil fraction (f_{NF}) for the winter samples (Fig. 6) exhibits high values, with mean values equal to 0.89 and 0.84 for Passy and Chamonix, respectively. Lower values observed at Passy in summer (mean $f_{NF} = 0.75$) indicate that the fossil component is more important in relative term to the total carbon content of aerosols, but that an important non-fossil fraction is still largely dominant.

The concentrations of non-fossil carbon (TC_{NF}) and fossil carbon (TC_F) can be calculated by multiplying the total carbon concentration (TC) by the non-fossil fraction (f_{NF}) and the fossil fraction (f_F), respectively.

While the mean TC is about 13 times larger in winter than summer, the fossil carbon concentration TC_F exhibits a smaller variation between seasons, as expected from similar traffic over the year. Nonetheless, the TC_F winter concentration is still about 3 times the summer one, which may be related to the reduced atmospheric dynamics during winter, leading to trapping of particles by the inversion layers.

Schmidl et al. (2008) demonstrated that combustion of five biomass fuel types (spruce, larch, beech, oak, and briquettes) at similar burning conditions leads to a wide range of total carbon to levoglucosan ratios, from 4.3 to 17.2. In their study, the TC only originates from wood combustion and can thus be considered as completely non-fossil TC. The mean TC_{NF} / levoglucosan ratios equal 6.2 (SD = 0.4, $N = 28$) for Passy and 6.0 (SD = 0.3, $N = 13$) for Chamonix. These ratios are within the range, but do not correspond to any particular wood type, as presented by Schmidl et al. (2008). However, the TC_{NF} / levoglucosan ratios for Chamonix and Passy are in good agreement with those obtained by Zotter et al. (2014) for several Swiss stations in the southern Alps with ratios close to 6.2 ± 2.0, with the exception of Chiasso station (TC_{NF} / levo ratio about 9.1 ± 2.6).

The TC_{NF} values are plotted against levoglucosan in Fig. 7, and show a linear relation with high correlation coefficients for Chamonix (Pearson's $r = 0.989$) and Passy (Pearson's $r = 0.995$) samples. Moreover, the intercepts are not statistically different from zero, showing that virtually all TC_{NF} during winter originates from the burning of biomass, and more specifically, from wood combustion used for heating.

One interesting point with these excellent correlations is their stability, considering the large array of samples, which may include samples with various aging histories and thus variable amounts of secondary aerosols produced from VOCs emitted during biomass combustion. Nevertheless, the correlations are established between a primary tracer (levoglucosan) and a total carbon quantity, which includes both primary and secondary carbonaceous aerosols. Therefore, the excellent correlation implies either that the primary particles are dominant (in general for the total emission or because the secondary formation is slow in our conditions) or that the fraction of secondary particles is constant in relative terms (i.e., the correlation would remain even if secondary particles were dominant).

As a purely hypothetical case, let us assume that secondary organic aerosols (SOA) vary between 25 and 50 % by OC mass of the primary organic aerosols (POA), according to VOC conversion kinetics (i.e., 25 % in a recent air and 50 % in an older one). The majority of carbonaceous aerosols would still be composed of primary aerosols, ranging from 80 to 67 % of the total carbon, for the two end-members.

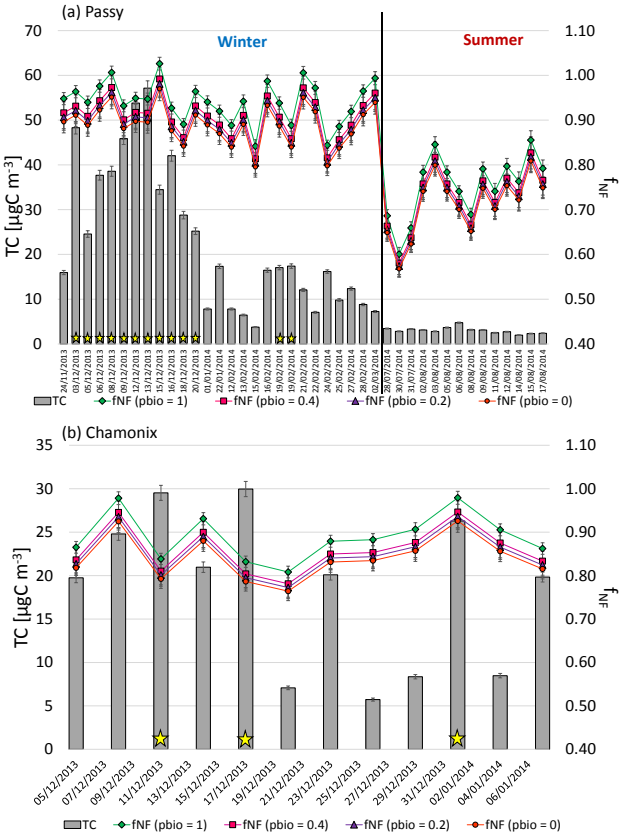

Figure 6. Results for **(a)** Passy and **(b)** Chamonix. Grey bars represent carbon concentration. Days with a PM_{10} concentration higher than 50 µg m^{-3} are marked with a yellow star. Green diamonds stand for the only biogenic f_{NFref}, pink squares are for f_{NFref} with a 40 % biogenic fraction, purple triangles denote f_{NFref} with a 20 % biogenic fraction, and red dots stand for f_{NFref} with a 0 % biogenic fraction. In all cases, the non-fossil fraction remains at very high levels during the winter season, validating the importance of the non-fossil source. A maximum variation of 6 % is observed in the different f_{NF} estimations.

However, because the dynamic range of total emissions is very large, this variability due to aerosol aging is difficult to detect on the TC_{NF} vs. levoglucosan diagram (Fig. 7).

Keeping the same educated guess would imply that for a particular levoglucosan concentration value, one could observe a 20 % range of TC_{NF} (i.e., 150/125 = 1.2). To illustrate this in Fig. 7, we show two extreme cases assuming only young air (i.e., SOA = 25 % of POA) or only older air (i.e., SOA = 50 % of POA). For the same value of levoglucosan, the TC_{NF} ratio between the two extremes should be 1.2, which can be approximated by decreasing or increasing the observed slope by about 10 % (dotted lines in Fig. 7) around the observed correlation assumed to be centered between the two end-members. Even if the observed correlation in Fig. 7 is strong, it is clear that its scatter is not completely negligible, but is within the variation between the two hypo-

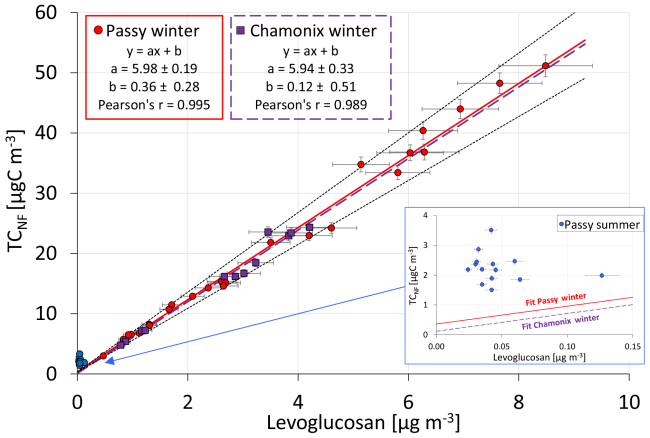

Figure 7. Comparison of TC_{NF}, based on ^{14}C / ^{12}C ratio measurements, with levoglucosan. TC_{NF} corresponds to the carbon concentration multiplied by the f_{NF}. For the winter samples, f_{NF} is determined for $p_{bio} = 0$ and for summer samples, $p_{bio} = 1$. It has to be underlined that a variation in p_{bio} does not affect the significance of the relationship between levoglucosan and TC_{NF} (see Table 5). Purple squares indicate Chamonix winter samples, red dots Passy winter samples, and blue dots denote Passy summer samples. Winter samples display very strong correlations between TC_{NF} and levoglucosan with close to zero intercepts, suggesting that virtually all of the TC_{NF} originates from biomass burning. The fit parameters have been calculated by taking into account both error bars on the x and y axes and are given with their 95 % confidence interval. Black dotted lines stand for two extreme cases assuming only young air (i.e., SOA = 25 % of POA) or only older air (i.e., SOA = 50 % of POA); see Sect. 3.2.1 for further information. No correlation is found for the summer samples, implying the summer TC_{NF} originates from other non-fossil sources.

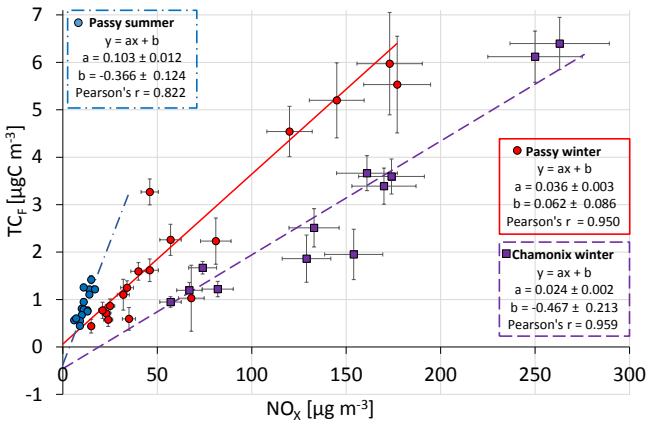

Figure 8. Comparison of TC_F, based on ^{14}C / ^{12}C ratio measurements, with NO_x. TC_F corresponds to the carbon concentration multiplied by f_F. For the winter samples, f_F is determined for $p_{bio} = 0$ and for summer samples $p_{bio} = 1$. It has to be underlined that a variation in p_{bio} does not affect the significance of the relationship between levoglucosan and TC_{NF} (see Table 5). Purple squares denote Chamonix winter samples, red dots denote Passy winter samples, and blue dots designate Passy summer samples. Each dataset exhibits a good correlation between NO_x and TC_F concentrations. The fit parameters have been calculated by taking into account both error bars on the x and y axes and are given with their 95 % confidence interval. A higher slope value is obtained for the summer datasets than for the winter ones, which suggests either different fossil carbon sources or NO_x degradation rate depending on the season.

thetical extremes (see for examples the TC_{NF} values corresponding to about 6 µg m^{-3} of levoglucosan). These observations and speculations would certainly justify specific studies on secondary aerosol formation processes in the atmospheric conditions of the Arve River valley.

During summer, domestic heating emissions are presumed to be weak, as confirmed by really low levoglucosan concentrations. Levoglucosan and TC_{NF} concentrations show no correlation for summer samples (represented by blue dots in Fig. 7). As mentioned above, TC_{NF} still represents on average 75 % of the total carbon in summer. It has already been demonstrated that the modern sources of carbon are dominant over the fossil fuel ones in atmospheric PM of many sites, even in a large city like Marseille, France (El Haddad et al., 2011). This is also the case in these more rural environments. These TC_{NF} levels are about 4 times higher than expected by the regression model determined for the winter samples if they were due to biomass burning. These results indicate that the main non-fossil sources differ between seasons. For the winter season, TC_{NF} is directly related to biomass burning, whereas during summer these sources are most probably biogenic emissions.

To attribute the fossil fraction of the carbonaceous particles, the concentrations of fossil carbon (TC_F) are plotted against NO_x concentration (Fig. 8), which is considered as a vehicle emission proxy. Linear correlations are highly statistically significant for all three different datasets. All origin intercepts are equivalent or close to zero. For winter datasets, the slope obtained for the French datasets are roughly equivalent to those given by Zotter et al. (2014) for the EC_F vs. NO_x correlations in many Swiss sites (no correlations were observed with OC_F in this last study). However, in our study, the slopes for Passy and Chamonix are clearly different, with that in Passy being 50 % higher. The reason for such a difference is currently unknown, but may be related to the vehicle fleet influencing the two sites: while the site in Chamonix is an urban traffic site with only passenger vehicles, the site in Passy is an urban background site 1 km away from the highway to Italy, which supports a large amount of international truck traffic. Also, the impact of some industrial emissions in Passy remains to be investigated.

The slope obtained for the summer samples (only in Passy) is larger than that obtained for winter, which may suggest different vehicular emissions in summer than in winter or an extensive degradation of NO_x during summer. Another hypothesis is that secondary formation of OC from vehicular

gaseous emissions may well be greater in summer than in winter.

3.2.2 Apportionment with biogenic fraction variations

The calculations above only constitute a first approximation that takes into account a single non-fossil source to define $f_{NF,ref}$. So far, we considered the non-fossil source to be purely biogenic during summer and to originate exclusively from biomass burning only during winter. However, the non-fossil carbon is made up of these two different fractions that differ slightly in their $^{14}C / ^{12}C$ ratios, and both have to be acknowledged in the definition of $f_{NF,ref}$.

Zhang et al. (2012) assumed a biogenic fraction (p_{bio}) constant throughout the year, implying that its origin does not vary with the season. More recently, Zotter et al. (2014) applied a variability with the seasons: the biogenic fraction is set at 0.4 during summer and 0.2 during winter since no large contributions from biogenic sources are expected during the cold season. With these two assumptions, the maximum $F^{14}C$ value in the absence of a fossil component is given by the following mass balance equation Eq. (7) (Szidat et al., 2006; Zhang et al., 2012; Zotter et al., 2014):

$$f_{NF,ref} = p_{bio} \times F^{14}C_{bio} + (1 - p_{bio}) \times F^{14}C_{bb}, \quad (7)$$

where $F^{14}C_{bio}$ and $F^{14}C_{bb}$ correspond to the $F^{14}C$ values of the biogenic (1.04) and the biomass burning components (1.10), respectively. Similarly, p_{bio} corresponds to the biogenic fraction in the total non-fossil carbon, whereas the biomass burning fraction is simply $(1 - p_{bio})$. Figure 6 shows the time series of the f_{NF} values calculated by using both the simple and sophisticated models for both sites. In all cases, it must be noted that introducing various values of p_{bio} has a minor impact on $f_{NF,ref}$. Indeed, a decrease of p_{bio} from 1 to 0 would change $f_{NF,ref}$ by 6 %. In the same way, the regression parameters for the TC_{NF} vs. levoglucosan correlations are listed in Table 5 for the different values of $f_{NF,ref}$ (i.e., with $p_{bio} = 1$, 0.4, 0.2, and 0). It can be seen that the small variation of $f_{NF,ref}$ has a negligible impact on the linear regression parameters. All approaches confirm the dominance of the biomass burning component during winter, as illustrated in Fig. 6.

Table 5 also provides all parameters for the TC_F vs. NO_x linear fits. Again, correlation coefficients are significant for all values of p_{bio} (1, 0.4, 0.2, and 0), confirming that introducing the hypotheses for this second model does not lead to changes in the source partitioning.

3.2.3 Apportionment for summer samples: independent determination of the non-fossil fraction

One inherent problem with the previous model is that it relies on a priori assumptions about the sources of the non-fossil fraction. In addition, it assumes that the biomass burning and biogenic concentrations (TC_{bb} and TC_{bio}) are proportional to TC_{NF}, which also implies a linear correlation between the two fractions, i.e., $TC_{bb} = [(1 - p_{bio})/p_{bio}] \times TC_{bio}$. Indeed, one could well imagine a variable emission of biomass burning superimposed on a rather constant emission of biogenic particles, or even a more complex situation as the two sources have different and rather independent origins.

In Sect. 3.2.1, the nearly exclusive contribution of biomass burning to the non-fossil fraction during winter has been demonstrated by the strong linear correlation between levoglucosan and TC_{NF} (Fig. 7 and Table 5) and by intercepts nearly equal to zero (i.e., $TC_{NF} \approx TC_{bb}$ during winter). For summer samples, the insert in Fig. 7 shows that the TC_{bb} expected by the linear models is lower than the measured TC_{NF}, suggesting another source of non-fossil carbon.

As an alternative model, we tentatively propose that the part of TC_{NF} due to biomass burning (TC_{bb}) in a particular sample could be calculated from its levoglucosan concentration by using its linear correlation to TC_{NF} observed in winter (i.e., $TC_{bb} = a \times$ [levoglucosan], a being the slope of the linear relationship shown in Fig. 7).

Total carbon (TC) is composed of both fossil TC_F and non-fossil fraction TC_{NF}. The latter can be subdivided into parts corresponding to the considered sources, i.e., biomass burning and biogenic emissions (TC_{bb} and TC_{bio}, respectively).

$$TC = TC_{NF} + TC_F = TC_{bb} + TC_{bio} + TC_F \quad (8)$$

This leads to the following ^{14}C mass balance:

$$\begin{aligned} TC \times F^{14}C_S &= TC_{bb} \times F^{14}C_{bb} + TC_{bio} \times F^{14}C_{bio} \\ &+ TC_F \times F^{14}C_F = TC_{bb} \times F^{14}C_{bb} \\ &+ TC_{bio} \times F^{14}C_{bio}, \end{aligned} \quad (9)$$

with $F^{14}C_S$ as the measured $^{14}C / ^{12}C$ ratio of the sample, $F^{14}C_{bb} = 1.10$, $F^{14}C_{bio} = 1.04$, and $F^{14}C_F = 0$ as previously discussed in Sect. 3.2.1. TC is the total carbon of the sample [$\mu g C\, m^{-3}$], TC_{bb} is the carbon originating from biomass burning, TC_{bio} is the carbon from biogenic emissions, and finally TC_F is the carbon from fossil sources.

It is thus possible to calculate the biogenic fraction and the fossil fraction by combining the ^{14}C mass balance in Eq. (10) and the total carbon mass balance in Eq. (11).

$$TC_{bio} = \frac{F^{14}C_S \times TC - TC_{bb} \times F^{14}C_{bb}}{F^{14}C_{bio}} \quad (10)$$

$$TC_F = TC - TC_{bb} - TC_{bio} \quad (11)$$

The results for summer samples are provided in Table 6. It should be stressed that this model relies on the hypothesis that levoglucosan does not suffer from a large differential degradation between summer and winter, which may be valid to a first order as PM sampling has been carried out close to the emission sources. The contribution of fossil carbon to TC is estimated to be about 25 %, corresponding to very low fossil carbon concentration, i.e., 0.80 $\mu g C\, m^{-3}$. By contrast, the

Table 5. Determination of the linear fit parameters (with their 95 % confidence intervals) for the linear relation between TC_{NF} and levoglucosan, and for the linear relation between TC_F and NO_x. Variation in p_{bio} and in TC_{NF} and TC_F does not have a major influence on the regression parameters in the case of TC_{NF} vs. Levoglucosan but does in the case of TC_F vs. NO_x because of the small amount of TC_F.

	TC_{NF} vs. Levoglucosan					TC_F vs. NO_x				
	a	$\pm a$	b	$\pm b$	Pearson's r	a	$\pm a$	b	$\pm b$	Pearson's r
Passy summer $p_{bio} = 1$	–	–	–	–	–	0.103	0.012	−0.366	0.124	0.822
Passy summer $p_{bio} = 0.4$	–	–	–	–	–	0.099	0.014	−0.270	0.145	0.813
Passy summer $p_{bio} = 0.2$	–	–	–	–	–	0.100	0.014	−0.259	0.145	0.809
Passy summer $p_{bio} = 0$	–	–	–	–	–	0.107	0.013	−0.284	0.132	0.806
Passy winter $p_{bio} = 1$	6.33	0.20	0.38	0.29	0.995	0.024	0.002	−0.040	0.063	0.782
Passy winter $p_{bio} = 0.4$	6.11	0.20	0.38	0.30	0.995	0.028	0.004	0.127	0.134	0.914
Passy winter $p_{bio} = 0.2$	6.04	0.20	0.37	0.30	0.995	0.031	0.004	0.129	0.133	0.935
Passy winter $p_{bio} = 0$	5.98	0.19	0.36	0.28	0.995	0.036	0.003	0.062	0.086	0.950
Chamonix winter $p_{bio} = 1$	6.29	0.35	0.12	0.54	0.989	0.019	0.002	−0.490	0.167	0.885
Chamonix winter $p_{bio} = 0.4$	6.06	0.35	0.13	0.55	0.989	0.021	0.003	−0.392	0.283	0.938
Chamonix winter $p_{bio} = 0.2$	6.00	0.35	0.13	0.54	0.989	0.023	0.003	−0.407	0.283	0.949
Chamonix winter $p_{bio} = 0$	5.94	0.33	0.12	0.51	0.989	0.024	0.002	−0.467	0.213	0.959

results point to a major contribution of about 87 % and up to 93 % of biogenic emissions to the non-fossil fraction (i.e., p_{bio} is about 0.9).

The biogenic carbon concentrations (TC_{bio}) can be compared to the concentrations of polyols as these sugar–alcohols are known to be tracers for primary biogenic aerosol particles (Yttri et al., 2007). As shown in Fig. 9, there is no simple relationship between TC_{bio} and polyols for the summer samples, indicating that despite its potential to be a large contributor to PM_{10} in some environments (Waked et al., 2014), this source may not be dominant in the modern fraction of carbon in summer in the Arve River valley.

TC_{bio} includes both primary and secondary organic aerosols, which result from the oxidation of biogenic volatile organic carbon compounds (BVOCs). It is known that BVOC emissions generally follow the temperature (Leaitch et al., 2011). Indeed, Fig. 10 shows that TC_{bio} increases with the mean temperature during the warmest part of the day (from 10:00 to 18:00 UTC + 01:00 for winter samples and UTC + 02:00 for summer samples) defining a significant linear correlation (Pearson's coefficient of 0.65 with a slope of 0.27 ± 0.05 and y intercept of -3.41 ± 1.06). Given the physiological effect of temperature, it is logical to expect that emissions are negligible at the low temperature, which can be

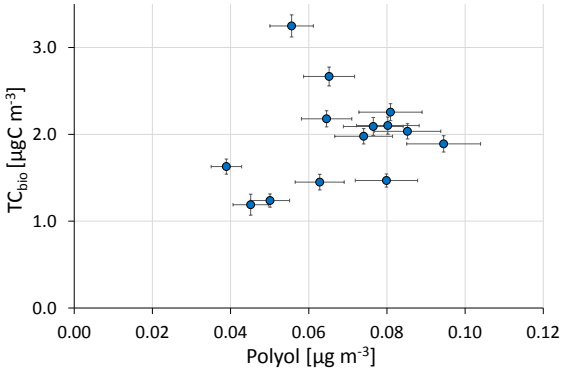

Figure 9. Comparison of TC_{bio} based on levoglucosan and ^{14}C / ^{12}C ratio measurements against polyol concentrations. Blue dots stand for the Passy summer samples. No correlation is found between TC_{bio} and polyol concentrations (primary biogenic emissions tracers). TC_{bio} could originate from secondary organic carbon from the oxidation of biogenic VOC.

Table 6. Results of summer samples from Passy. TC_{bb} is calculated from levoglucosan concentration. TC_{bio} and TC_F come out from TC_{bb} and the $F^{14}C$ of the sample. TC_{NF} / TC and TC_F / TC are equivalent to f_{NF} and f_F determined directly by ^{14}C measurements. The major part of TC_{NF} is composed of TC_{bio}. The uncertainties represent the confidence intervals (95 %) and are determined by uncertainties propagation.

Date dd/mm/yyyy	TC_{bb} [µgC m^{-3}]	$\pm TC_{bb}$ [µgC m^{-3}]	TC_{bio} [µgC m^{-3}]	$\pm TC_{bio}$ [µgC m^{-3}]	TC_F [µgC m^{-3}]	$\pm TC_F$ [µgC m^{-3}]	TC_{NF} / TC	TC_F / TC	TC_{bio} / TC_{NF}	polyol [ng m^{-3}]	$\pm$polyol [ng m^{-3}]
28/07/2014	0.18	0.02	2.18	0.09	1.09	0.15	0.68	0.32	0.92	64.56	6.46
30/07/2014	0.21	0.02	1.47	0.08	1.14	0.12	0.60	0.40	0.88	79.88	7.99
31/07/2014	0.21	0.02	1.98	0.09	1.15	0.14	0.66	0.34	0.90	74.04	7.40
02/08/2014	0.18	0.02	2.26	0.10	0.69	0.14	0.78	0.22	0.92	80.91	8.09
03/08/2014	0.26	0.03	2.10	0.10	0.45	0.14	0.84	0.16	0.89	80.23	8.02
05/08/2014	0.19	0.02	2.67	0.11	0.80	0.16	0.78	0.22	0.93	65.20	6.52
06/08/2014	0.25	0.03	3.25	0.13	1.24	0.20	0.74	0.26	0.93	55.61	5.56
08/08/2014	0.14	0.02	2.03	0.09	1.00	0.14	0.69	0.31	0.93	85.26	8.53
09/08/2014	0.36	0.04	2.09	0.10	0.67	0.15	0.78	0.22	0.85	76.51	7.65
11/08/2014	0.38	0.04	1.45	0.09	0.67	0.13	0.73	0.27	0.79	62.80	6.28
12/08/2014	0.27	0.03	1.89	0.09	0.57	0.14	0.79	0.21	0.87	94.51	9.45
14/08/2014	0.25	0.03	1.24	0.08	0.48	0.11	0.76	0.24	0.83	50.09	5.01
15/08/2014	0.76	0.08	1.19	0.12	0.38	0.17	0.84	0.16	0.61	45.14	4.51
17/08/2014	0.25	0.03	1.63	0.09	0.51	0.13	0.79	0.21	0.87	38.93	3.89

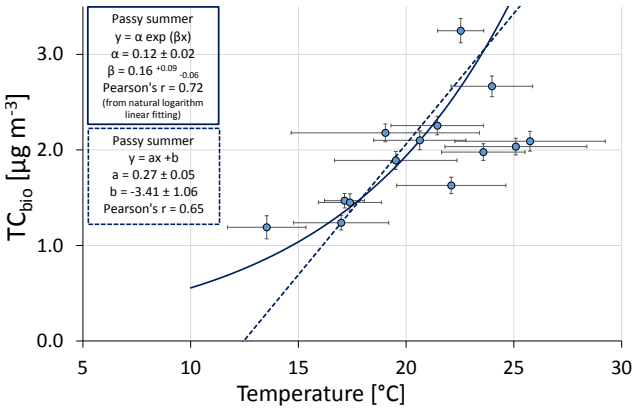

Figure 10. Comparison of TC_{bio} based on levoglucosan and ^{14}C / ^{12}C ratio measurements plotted vs. the average temperature of the warmest part of the day (10:00 to 18:00 UTC + 02:00). Blue dots stand for the Passy summer samples. TC_{bio} concentration increases with the temperature. Both linear (dashed line) and exponential (solid line) relations are represented with their correlation coefficient. The fit parameters have been calculated by taking into account both error bars on the x and y axes and are given with their 95 % confidence interval. The exponential fit is preferred as the TC_{bio} emission cannot be negative. Moreover, emission of BVOCs (precursors of SOA) emission rate is classically described with an exponential law (Leaitch et al., 2011).

approximated by an exponential law given in Eq. (12) as in Leaitch et al. (2011).

$$TC_{bio} = \alpha \times \exp(\beta \times T), \quad (12)$$

where T is expressed in degrees Celsius, α is a constant, which could be assimilated to a base capacity, and β is an empirical constant. By studying the linear correlation between $\ln(TC_{bio})$ and temperature, it is possible to calculate $\alpha = 0.12 \pm 0.02$ and $\beta = 0.16$ $(+0.09/-0.06)$, with a Pearson's coefficient of 0.72. The correlation coefficient is thus slightly higher for the exponential law than for the linear model. In any case, the fact that TC_{bio} depends on temperature suggests that this fraction is mainly composed of secondary organic aerosol.

4 Conclusions

Quantifying the relative contribution of fossil and non-fossil sources of carbonaceous aerosols is important in order to better understand the sources of atmospheric particles and to attribute them to natural and anthropogenic processes. For example, both biomass burning for domestic heating and road traffic emissions are known to contribute to PM pollution in many urban areas, notably in the Arve River valley (French Alps), which is the focus of this study.

Radiocarbon (^{14}C) analysis is the best way to distinguish fossil fuel combustion products from other carbon sources

such as biomass burning and biogenic emissions. We show here that ^{14}C is efficiently measured in aerosol samples with the AixMICADAS spectrometer by using an elemental analyzer (EA) coupled to its CO_2 gas ion source, which can handle small samples (10–100 µgC). This direct coupling avoids the production of solid graphite targets, which is the usual bottleneck in traditional radiocarbon measurement by accelerator mass spectrometry. The present work leads to the following conclusions:

- Contamination of the measurement procedure is mainly linked to the silver boats in which the filter samples are wrapped prior to combustion in the EA. This contamination has been quantified and shown to be fairly constant, which enables rectification of the measurements of aerosol samples.

- The precision and accuracy of ^{14}C measurements in aerosols are validated over the full range of expected fossil and non-fossil carbon values by using various standards and synthetic mixtures.

- Carbon concentrations of aerosols determined by thermal-optical analysis (LGGE in Grenoble) and GIS quantification (CEREGE in Aix-en-Provence) in samples from Passy and Chamonix are in excellent agreement and indicate large concentrations of up to 50 µgC m^{-3} during winters.

- Mean winter carbon concentrations are higher than those reported for several urban sites but are in the range of those measured in other Alpine sites.

- Levoglucosan content is used as a biomass burning proxy, indicating very high levels during winter with values of up to 8 µg m^{-3} in Passy, thus higher than those generally observed in several European cities.

- Based on ^{14}C measurements, the fractions of non-fossil carbon determined in winter (0.89 for Passy and 0.84 for Chamonix) are higher than the non-fossil fraction obtained for Passy during summer (0.75). However, the non-fossil fraction remains dominant during summer with a fossil contribution of about 25 %, probably from road traffic.

- Non-fossil carbon concentration (TC_{NF}) is strongly correlated with levoglucosan concentration for winter samples (Passy and Chamonix). The linear regression intercepts are close to zero suggesting that almost all of the non-fossil carbon originates from biomass burning and more specifically from wood combustion used for heating during the winter.

- Fossil carbon concentrations exhibit a strong correlation with NO_x concentrations, suggesting that the source of fossil carbon is directly linked to traffic emissions.

- Summer samples exhibit an important relative contribution of non-fossil sources (75 %). A dual approach based on ^{14}C and levoglucosan enables the calculation of a first estimation of the biogenic and biomass burning fractions in the non-fossil carbon. The samples from Passy allow to test this new model, suggesting that for this site the biogenic emissions are the most important contributor to the non-fossil fraction during summer.

- The lack of correlation between polyols (tracers of biogenic activity in soil) and the biogenic fraction suggests that TC_{bio} could be composed of secondary organic aerosols resulting from the oxidation of biogenic VOC, which is also suggested by the correlation between TC_{bio} and temperature.

  Overall, combining radiocarbon and levoglucosan measurements strengthens findings concerning the dominant contribution of winter biomass burning to aerosols in the Arve River valley. In addition to first-order agreement, both tracers are complementary: levoglucosan enables the identification of the source while ^{14}C allows the precise quantification of the fossil and non-fossil fractions.

  We show that this dual approach may also serve to go further in quantifying these additional carbon sources. Combining ^{14}C and levoglucosan measurements allows reconstruction of other contributions such as biogenic aerosols fluxes. As an example, our new model is applied to summer samples from Passy leading to reasonable evaluations of biogenic particle fluxes. These aerosols are probably linked to oxidation of volatile organic compounds (VOCs) as suggested by a significant correlation of fluxes with temperature.

  Following Zhang et al. (2012), ongoing research at CEREGE into ^{14}C measurements of separated elemental carbon and organic carbon fractions of aerosol should provide more precise source apportionment in the future.

5 Data availability

Detailed data are available as a Supplement.

The Supplement related to this article is available online at doi:10.5194/acp-16-13753-2016-supplement.

Acknowledgements. AixMICADAS was acquired and is operated in the framework of the EQUIPEX project ASTER-CEREGE (PI E. Bard) with additional matching funds from the Collège de France, which also supports the salaries of the authors from CEREGE. We thank Sönke Szidat for advice on reporting ^{14}C results on aerosols.

Edited by: W. Maenhaut
Reviewed by: three anonymous referees

References

Aymoz, G., Jaffrezo, J. L., Chapuis, D., Cozic, J., and Maenhaut, W.: Seasonal variation of PM_{10} main constituents in two valleys of the French Alps. I: EC / OC fractions, Atmos. Chem. Phys., 7, 661–675, doi:10.5194/acp-7-661-2007, 2007.

Bard, E., Tuna, T., Fagault, Y., Bonvalot, L., Wacker, L., Fahrni, S., and Synal, H.-A.: AixMICADAS, the accelerator mass spectrometer dedicated to ^{14}C recently installed in Aix-en-Provence, France, Nucl. Instrum. Meth. B, 361, 80–86, doi:10.1016/j.nimb.2015.01.075, 2015.

Bauer, H., Claeys, M., Vermeylen, R., Schueller, E., Weinke, G., Berger, A., and Puxbaum, H.: Arabitol and mannitol as tracers for the quantification of airborne fungal spores, Atmos. Environ., 42, 588–593, doi:10.1016/j.atmosenv.2007.10.013, 2008.

Birch, M. E. and Cary, R. A.: Elemental carbon-based method for monitoring occupational exposures to particulate diesel exhaust, Aerosol Sci. Tech., 25, 221–241, doi:10.1080/02786829608965393, 1996.

Bond, T. C., Doherty, S. J., Fahey, D. W., Forster, P. M., Berntsen, T., DeAngelo, B. J., Flanner, M. G., Ghan, S., Kärcher, B., Koch, D., Kinne, S., Kondo, Y., Quinn, P. K., Sarofim, M. C., Schultz, M. G., Schulz, M., Venkataraman, C., Zhang, H., Zhang, S., Bellouin, N., Guttikunda, S. K., Hopke, P. K., Jacobson, M. Z., Kaiser, J. W., Klimont, Z., Lohmann, U., Schwarz, J. P., Shindell, D., Storelvmo, T., Warren, S. G., and Zender, C. S.: Bounding the role of black carbon in the climate system: A scientific assessment, J. Geophys. Res.-Atmos., 118, 5380–5552, doi:10.1002/jgrd.50171, 2013.

Caseiro, A., Bauer, H., Schmidl, C., Pio, C. A., and Puxbaum, H.: Wood burning impact on PM_{10} in three Austrian regions, Atmos. Environ., 43, 2186–2195, doi:10.1016/j.atmosenv.2009.01.012, 2009.

Cavalli, F., Viana, M., Yttri, K. E., Genberg, J., and Putaud, J.-P.: Toward a standardised thermal-optical protocol for measuring atmospheric organic and elemental carbon: the EUSAAR protocol, Atmos. Meas. Tech., 3, 79–89, doi:10.5194/amt-3-79-2010, 2010.

Cavanagh, R. R. and Watters, R. L.: Report of investigation Reference Material 8785 air particulate matter on filter media (a fine fraction of SRM1649a Urban Dust on quartz-fiber filter), National Institute of Standards & Technology, Gaithersburg, MD, 22 pp., 2005.

Chevrier, F., Brulfert, G., Mocnik, G., Marchand, N., Jaffrezo, J.-L., and Besombes, J.-L.: DECOMBIO – Contribution de la combustion de la biomasse aux PM_{10} en vallée de l'Arve: mise en place et qualification d'un dispositif de suivi, Poll. Atmos., in press, 2016.

Chung, S. H. and Seinfeld, J. H.: Global distribution and climate forcing of carbonaceous aerosols, J. Geophys. Res.-Atmos., 107, 4407, doi:10.1029/2001JD001397, 2002.

Currie, L. A. and Kessler, J. D.: On the isolation of elemental carbon (EC) for micro-molar ^{14}C accelerator mass spectrometry: development of a hybrid reference material for ^{14}C-EC accuracy assurance, and a critical evaluation of the thermal optical kinetic (TOK) EC isolation procedure, Atmos. Chem. Phys., 5, 2833–2845, doi:10.5194/acp-5-2833-2005, 2005.

Currie, L. A., Klouda, G. A., and Voorhees, K. J.: Atmospheric carbon: The importance of accelerator mass spectrometry, Nucl. Instrum. Meth. B, 5, 371–379, doi:10.1016/0168-583X(84)90544-5, 1984.

Currie, L. A., Stafford, T. W., Sheffield, A. E., Klouda, G. A., Wise, S. A., Fletcher, R. A., Donahue, D. J., Jull, A. J. T., and Linick, T. W.: Microchemical and molecular dating, Radiocarbon, 31, 448–463, 1989.

Currie, L. A., Benner Jr., B. A., Kessler, J. D., Klinedinst, D. B., Klouda, G. A., Marolf, J. V., Slater, J. F., Wise, S. A., Cachier, H., Cary, R., Chow, J. C., Watson, J., Druffel, E. R. M., Masiello, C. A., Eglinton, T. I., Pearson, A., Reddy, C. M., Gustafsson, O., Hartmann, P. C., Quinn, J. G., Hedges, J. I., Prentice, K. M., Kirchstetter, T. W., Novakov, T., Puxbaum, H., and Schmid, H.: A critical evaluation of interlaboratory data on total, elemental, and isotopic carbon in the carbonaceous particle reference material, NIST SRM 1649a, J. Res. Natl. Inst. Stan., 107, 279–298, 2002.

El Haddad, I., Marchand, N., Wortham, H., Piot, C., Besombes, J.-L., Cozic, J., Chauvel, C., Armengaud, A., Robin, D., and Jaffrezo, J.-L.: Primary sources of $PM_{2.5}$ organic aerosol in an industrial Mediterranean city, Marseille, Atmos. Chem. Phys., 11, 2039–2058, doi:10.5194/acp-11-2039-2011, 2011.

Engling, G., Carrico, C. M., Kreidenweis, S. M., Collett Jr., J. L., Day, D. E., Malm, W. C., Lincoln, E., Min Hao, W., Iinuma, Y., and Herrmann, H.: Determination of levoglucosan in biomass combustion aerosol by high-performance anion-exchange chromatography with pulsed amperometric detection, Atmos. Environ., 40, 299–311, doi:10.1016/j.atmosenv.2005.12.069, 2006.

Eriksson-Stenström, K., Skog, G., Georgiadou, E., Genberg, J., and Mellström, A.: A guide to radiocarbon units and calculations, Lund University, Sweden, 18 pp., 2011.

Fahrni, S. M., Wacker, L., Synal, H.-A., and Szidat, S.: Improving a gas ion source for ^{14}C AMS, Nucl. Instrum. Meth. B, 294, 320–327, doi:10.1016/j.nimb.2012.03.037, 2013.

Favez, O., El Haddad, I., Piot, C., Boréave, A., Abidi, E., Marchand, N., Jaffrezo, J.-L., Besombes, J.-L., Personnaz, M.-B., Sciare, J., Wortham, H., George, C., and D'Anna, B.: Inter-comparison of source apportionment models for the estimation of wood burning aerosols during wintertime in an Alpine city (Grenoble, France), Atmos. Chem. Phys., 10, 5295–5314, doi:10.5194/acp-10-5295-2010, 2010.

Genberg, J., Stenström, K., Elfman, M., and Olsson, M.: Sealed glass tube combustion of µg-sized aerosol samples, Lund University, Radiocarbon, 52, 1270–1276, 2010.

Genberg, J., Perron, N., Olsson, M., and Stenstrom, K.: Sealed glass tube combustion of µg-sized aerosol samples, Radiocarbon, 55, 617–623, 2013.

Guenther, A., Hewitt, C. N., Erickson, D., Fall, R., Geron, C., Graedel, T., Harley, P., Klinger, L., Lerdau, M., Mckay, W. A., Pierce, T., Scholes, B., Steinbrecher, R., Tallamraju, R., Taylor, J., and Zimmerman, P.: A global model of natural volatile organic compound emissions, J. Geophys. Res.-Atmos., 100, 8873–8892, doi:10.1029/94JD02950, 1995.

Gustafsson, Ö., Kruså, M., Zencak, Z., Sheesley, R. J., Granat, L., Engström, E., Praveen, P. S., Rao, P. S. P., Leck, C., and Rodhe, H.: Brown clouds over South Asia: biomass or fossil fuel com-

bustion?, Science, 323, 495–498, doi:10.1126/science.1164857, 2009.

Heal, M. R., Naysmith, P., Cook, G. T., Xu, S., Duran, T. R., and Harrison, R. M.: Application of ^{14}C analyses to source apportionment of carbonaceous $PM_{2.5}$ in the UK, Atmos. Environ., 45, 2341–2348, doi:10.1016/j.atmosenv.2011.02.029, 2011.

Hennigan, C. J., Sullivan, A. P., Collett, J. L., and Robinson, A. L.: Levoglucosan stability in biomass burning particles exposed to hydroxyl radicals, Geophys. Res. Lett., 37, L09806, doi:10.1029/2010GL043088, 2010.

Herich, H., Gianini, M. F. D., Piot, C., Močnik, G., Jaffrezo, J.-L., Besombes, J.-L., Prévôt, A. S. H., and Hueglin, C.: Overview of the impact of wood burning emissions on carbonaceous aerosols and PM in large parts of the Alpine region, Atmos. Environ., 89, 64–75, doi:10.1016/j.atmosenv.2014.02.008, 2014.

Hua, Q., Barbetti, M., and Rakowski, A. Z.: Atmospheric Radiocarbon for the Period 1950–2010, Radiocarbon, 55, 2059–2072, doi:10.2458/azu_js_rc.v55i2.16177, 2013.

Jacobson, M. C., Hansson, H.-C., Noone, K. J., and Charlson, R. J.: Organic atmospheric aerosols: Review and state of the science, Rev. Geophys., 38, 267–294, doi:10.1029/1998RG000045, 2000.

Jerrett, M., Burnett, R. T., Ma, R., Pope, C. A., Krewski, D., Newbold, K. B., Thurston, G., Shi, Y., Finkelstein, N., Calle, E. E., and Thun, M. J.: Spatial analysis of air pollution and mortality in Los Angeles, Epidemiol. Camb. Mass, 16, 727–736, 2005.

Jordan, T. B., Seen, A. J., and Jacobsen, G. E.: Levoglucosan as an atmospheric tracer for woodsmoke, Atmos. Environ., 40, 5316–5321, doi:10.1016/j.atmosenv.2006.03.023, 2006a.

Jordan, T. B., Seen, A. J., Jacobsen, G. E., and Gras, J. L.: Radiocarbon determination of woodsmoke contribution to air particulate matter in Launceston, Tasmania, Atmos. Environ., 40, 2575–2582, doi:10.1016/j.atmosenv.2005.12.024, 2006b.

Kennedy, I. M.: The health effects of combustion-generated aerosols, P. Combust. Inst., 31, 2757–2770, doi:10.1016/j.proci.2006.08.116, 2007.

Kessler, S. H., Smith, J. D., Che, D. L., Worsnop, D. R., Wilson, K. R., and Kroll, J. H.: Chemical sinks of organic aerosol: kinetics and products of the heterogeneous oxidation of erythritol and levoglucosan, Environ. Sci. Technol., 44, 7005–7010, doi:10.1021/es101465m, 2010.

Klouda, G. A., Filliben, J. J., Parish, H. J., Chow, J. C., Watson, J. G., and Cary, R. A.: Reference Material 8785: air particulate matter on filter media, Aerosol Sci. Tech., 39, 173–183, doi:10.1080/027868290916453, 2005.

Leaitch, W. R., Macdonald, A. M., Brickell, P. C., Liggio, J., Sjostedt, S. J., Vlasenko, A., Bottenheim, J. W., Huang, L., Li, S.-M., Liu, P. S. K., Toom-Sauntry, D., Hayden, K. A., Sharma, S., Shantz, N. C., Wiebe, H. A., Zhang, W., Abbatt, J. P. D., Slowik, J. G., Chang, R. Y.-W., Russell, L. M., Schwartz, R. E., Takahama, S., Jayne, J. T., and Ng, N. L.: Temperature response of the submicron organic aerosol from temperate forests, Atmos. Environ., 45, 6696–6704, doi:10.1016/j.atmosenv.2011.08.047, 2011.

Lee, T., Sullivan, A. P., Mack, L., Jimenez, J. L., Kreidenweis, S. M., Onasch, T. B., Worsnop, D. R., Malm, W., Wold, C. E., Hao, W. M., and Collett, J. L. Jr.: Chemical smoke marker emissions during flaming and smoldering phases of laboratory open burning of wildland fuels, Aerosol Sci. Tech., 44, i–v, doi:10.1080/02786826.2010.499884, 2010.

Lelieveld, J., Evans, J. S., Fnais, M., Giannadaki, D., and Pozzer, A.: The contribution of outdoor air pollution sources to premature mortality on a global scale, Nature, 525, 367–371, doi:10.1038/nature15371, 2015.

Levin, I. and Kromer, B.: The tropospheric $^{14}CO_2$ level in mid-latitudes of the Northern Hemisphere (1959–2003), Radiocarbon, 46, 1261–1272, doi:10.1017/S0033822200033130, 2004.

Levin, I., Naegler, T., Kromer, B., Diehl, M., Francey, R. J., Gomez-Pelaez, A. J., Steele, L. P., Wagenbach, D., Weller, R., and Worthy, D. E.: Observations and modelling of the global distribution and long-term trend of atmospheric $^{14}CO_2$, Tellus B, 62, 26–46, doi:10.1111/j.1600-0889.2009.00446.x, 2010.

Levin, I., Kromer, B., and Hammer, S.: Atmospheric $\Delta^{14}CO_2$ trend in Western European background air from 2000 to 2012, Tellus B, 65, 20092, doi:10.3402/tellusb.v65i0.20092, 2013.

Lewis, C. W., Klouda, G. A., and Ellenson, W. D.: Radiocarbon measurement of the biogenic contribution to summertime $PM_{2.5}$ ambient aerosol in Nashville, TN, Atmos. Environ., 38, 6053–6061, doi:10.1016/j.atmosenv.2004.06.011, 2004.

Liu, D., Li, J., Zhang, Y., Xu, Y., Liu, X., Ding, P., Shen, C., Chen, Y., Tian, C., and Zhang, G.: The use of levoglucosan and radiocarbon for source apportionment of $PM_{2.5}$ carbonaceous aerosols at a background site in East China, Environ. Sci. Technol., 47, 10454–10461, doi:10.1021/es401250k, 2013.

Marchand, N., Besombes, J. L., Chevron, N., Masclet, P., Aymoz, G., and Jaffrezo, J. L.: Polycyclic aromatic hydrocarbons (PAHs) in the atmospheres of two French alpine valleys: sources and temporal patterns, Atmos. Chem. Phys., 4, 1167–1181, doi:10.5194/acp-4-1167-2004, 2004.

Penner, J. E., Chuang, C. C., and Grant, K.: Climate forcing by carbonaceous and sulfate aerosols, Clim. Dynam., 14, 839–851, doi:10.1007/s003820050259, 1998.

Pope, C. A. I. and Dockery, D. W.: Health effects of fine particulate air pollution: lines that connect, J. Air Waste Manage., 56, 709–742, doi:10.1080/10473289.2006.10464485, 2006.

Pöschl, U.: Atmospheric aerosols: composition, transformation, climate and health effects, Angew. Chem. Int. Ed., 44, 7520–7540, doi:10.1002/anie.200501122, 2005.

Putaud, J.-P., Raes, F., Van Dingenen, R., Brüggemann, E., Facchini, M.-C., Decesari, S., Fuzzi, S., Gehrig, R., Hüglin, C., Laj, P., Lorbeer, G., Maenhaut, W., Mihalopoulos, N., Müller, K., Querol, X., Rodriguez, S., Schneider, J., Spindler, G., ten Brink, H., Tørseth, K., and Wiedensohler, A.: A European aerosol phenomenology – 2: chemical characteristics of particulate matter at kerbside, urban, rural and background sites in Europe, Atmos. Environ., 38, 2579–2595, doi:10.1016/j.atmosenv.2004.01.041, 2004.

Putaud, J.-P., Van Dingenen, R., Alastuey, A., Bauer, H., Birmili, W., Cyrys, J., Flentje, H., Fuzzi, S., Gehrig, R., Hansson, H. C., Harrison, R. M., Herrmann, H., Hitzenberger, R., Hüglin, C., Jones, A. M., Kasper-Giebl, A., Kiss, G., Kousa, A., Kuhlbusch, T. A. J., Löschau, G., Maenhaut, W., Molnar, A., Moreno, T., Pekkanen, J., Perrino, C., Pitz, M., Puxbaum, H., Querol, X., Rodriguez, S., Salma, I., Schwarz, J., Smolik, J., Schneider, J., Spindler, G., ten Brink, H., Tursic, J., Viana, M., Wiedensohler, A., and Raes, F.: A European aerosol phenomenology – 3: Physical and chemical characteristics of particulate matter from 60 rural, urban, and kerbside sites across Europe, Atmos. Environ., 44, 1308–1320, doi:10.1016/j.atmosenv.2009.12.011, 2010.

Puxbaum, H., Caseiro, A., Sánchez-Ochoa, A., Kasper-Giebl, A., Claeys, M., Gelencsér, A., Legrand, M., Preunkert, S., and Pio, C.: Levoglucosan levels at background sites in Europe for assessing the impact of biomass combustion on the European aerosol background, J. Geophys. Res.-Atmos., 112, D23S05, doi:10.1029/2006JD008114, 2007.

Ramanathan, V., Crutzen, P. J., Kiehl, J. T., and Rosenfeld, D.: Aerosols, climate, and the hydrological cycle, Science, 294, 2119–2124, doi:10.1126/science.1064034, 2001a.

Ramanathan, V., Crutzen, P. J., Lelieveld, J., Mitra, A. P., Althausen, D., Anderson, J., Andreae, M. O., Cantrell, W., Cass, G. R., Chung, C. E., Clarke, A. D., Coakley, J. A., Collins, W. D., Conant, W. C., Dulac, F., Heintzenberg, J., Heymsfield, A. J., Holben, B., Howell, S., Hudson, J., Jayaraman, A., Kiehl, J. T., Krishnamurti, T. N., Lubin, D., McFarquhar, G., Novakov, T., Ogren, P. K., Podgorny, I. A., Prather, K., Priestley, K., Prospero, J. M., Quinn, P. K., Rajeev, K., Rasch, P., Rupert, S., Sadourny, R., Satheesh, S. K., Shaw, G. E., Sheridan, P., and Valero, F. P. J.: Indian Ocean Experiment: An integrated analysis of the climate forcing and effects of the great Indo-Asian haze, J. Geophys. Res., 106, 28371–28398, 2001b.

Reimer, P. J., Brown, T. A., and Reimer, R. W.: Discussion: reporting and calibration of post-bomb ^{14}C data, Radiocarbon, 46, 1299–1304, doi:10.1017/S0033822200033154, 2004.

Ruff, M., Szidat, S., Gäggeler, H. W., Suter, M., Synal, H.-A., and Wacker, L.: Gaseous radiocarbon measurements of small samples, Nucl. Instrum. Meth. B, 268, 790–794, doi:10.1016/j.nimb.2009.10.032, 2010a.

Ruff, M., Fahrni, S., Gäggeler, H. W., Hajdas, I., Suter, M., Synal, H.-A., Szidat, S., and Wacker, L.: On-line radiocarbon measurements of small samples using elemental analyser and MICADAS gas ion source, Radiocarbon, 52, 1645–1656, 2010b.

Salazar, G., Zhang, Y. L., Agrios, K., and Szidat, S.: Development of a method for fast and automatic radiocarbon measurement of aerosol samples by online coupling of an elemental analyzer with a MICADAS AMS, Nucl. Instrum. Meth. B, 361, 163–167, doi:10.1016/j.nimb.2015.03.051, 2015.

Schauer, J. J., Kleeman, M. J., Cass, G. R., and Simoneit, B. R. T.: Measurement of emissions from air pollution sources. 3. C1–C29 Organic compounds from meat charbroiling, Environ. Sci. Technol., 33, 1566–1577, doi:10.1021/es980076j, 1999.

Schauer, J. J., Kleeman, M. J., Cass, G. R., and Simoneit, B. R. T.: Measurement of emissions from air pollution sources. 3. C1–C29 Organic compounds from fireplace combustion of wood, Environ. Sci. Technol., 35, 1716–1728, doi:10.1021/es001331e, 2001.

Schmidl, C., Marr, I. L., Caseiro, A., Kotianová, P., Berner, A., Bauer, H., Kasper-Giebl, A., and Puxbaum, H.: Chemical characterisation of fine particle emissions from wood stove combustion of common woods growing in mid-European Alpine regions, Atmos. Environ., 42, 126–141, doi:10.1016/j.atmosenv.2007.09.028, 2008.

Simoneit, B. R. T., Schauer, J. J., Nolte, C. G., Oros, D. R., Elias, V. O., Fraser, M. P., Rogge, W. F., and Cass, G. R.: Levoglucosan, a tracer for cellulose in biomass burning and atmospheric particles, Atmos. Environ., 33, 173–182, doi:10.1016/S1352-2310(98)00145-9, 1999.

Stuiver, M.: International agreements and the use of the new oxalic acid standard, Radiocarbon, 25, 793–795, 1983.

Synal, H.-A., Stocker, M., and Suter, M.: MICADAS: A new compact radiocarbon AMS system, Nucl. Instrum. Meth. B, 259, 7–13, doi:10.1016/j.nimb.2007.01.138, 2007.

Szidat, S., Jenk, T. M., Gäggeler, H. W., Synal, H.-A., Hajdas, I., Bonani, G., and Saurer, M.: THEODORE, a two-step heating system for the EC / OC determination of radiocarbon (^{14}C) in the environment, Nucl. Instrum. Meth. B, 223–224, 829–836, doi:10.1016/j.nimb.2004.04.153, 2004.

Szidat, S., Jenk, T. M., Synal, H.-A., Kalberer, M., Wacker, L., Hajdas, I., Kasper-Giebl, A., and Baltensperger, U.: Contributions of fossil fuel, biomass-burning, and biogenic emissions to carbonaceous aerosols in Zurich as traced by ^{14}C, J. Geophys. Res.-Atmos., 111, D07206, doi:10.1029/2005JD006590, 2006.

Szidat, S., Prévôt, A. S. H., Sandradewi, J., Alfarra, M. R., Synal, H.-A., Wacker, L., and Baltensperger, U.: Dominant impact of residential wood burning on particulate matter in Alpine valleys during winter, Geophys. Res. Lett., 34, L05820, doi:10.1029/2006GL028325, 2007.

Szidat, S., Ruff, M., Perron, N., Wacker, L., Synal, H.-A., Hallquist, M., Shannigrahi, A. S., Yttri, K. E., Dye, C., and Simpson, D.: Fossil and non-fossil sources of organic carbon (OC) and elemental carbon (EC) in Göteborg, Sweden, Atmos. Chem. Phys., 9, 1521–1535, doi:10.5194/acp-9-1521-2009, 2009.

Szidat, S., Bench, G., Bernardoni, V., Calzolai, G., Czimczik, C. I., Derendorp, L., Dusek, U., Elder, K., Fedi, M., Genberg, J., Gustafsson, Ö., Kirillova, E., Kondo, M., McNichol, A. P., Perron, N., dos Santos, G. M., Stenström, K., Swietlicki, E., Uchida, M., Vecchi, R., Wacker, L., Zhang, Y., and Prévôt, A. S. H.: Intercomparison of ^{14}C analysis of carbonaceous aerosols: exercise 2009, Radiocarbon, 55, doi:10.2458/azu_js_rc.55.16314, 2013.

Uchida, M., Kumata, H., Koike, Y., Tsuzuki, M., Uchida, T., Fujiwara, K., and Shibata, Y.: Radiocarbon-based source apportionment of black carbon (BC) in PM_{10} aerosols from residential area of suburban Tokyo, Nucl. Instrum. Meth. B, 268, 1120–1124, doi:10.1016/j.nimb.2009.10.114, 2010.

Wacker, L., Němec, M., and Bourquin, J.: A revolutionary graphitisation system: fully automated, compact and simple, Nucl. Instrum. Meth. B, 268, 931–934, doi:10.1016/j.nimb.2009.10.067, 2010.

Wacker, L., Fahrni, S. M., Hajdas, I., Molnar, M., Synal, H.-A., Szidat, S., and Zhang, Y. L.: A versatile gas interface for routine radiocarbon analysis with a gas ion source, Nucl. Instrum. Meth. B, 294, 315–319, doi:10.1016/j.nimb.2012.02.009, 2013.

Waked, A., Favez, O., Alleman, L. Y., Piot, C., Petit, J.-E., Delaunay, T., Verlinden, E., Golly, B., Besombes, J.-L., Jaffrezo, J.-L., and Leoz-Garziandia, E.: Source apportionment of PM_{10} in a north-western Europe regional urban background site (Lens, France) using positive matrix factorization and including primary biogenic emissions, Atmos. Chem. Phys., 14, 3325–3346, doi:10.5194/acp-14-3325-2014, 2014.

Wise, S. A. and Watters, R. L. J.: Certificate of analysis, Standard Reference Material 1649a: Urban Dust, National Institute of Standards & Technology, Gaithersburg, MD, 24 pp., 2007.

Wise, S. A. and Watters, R. L. J.: Certificate of analysis, Standard Reference Material 1649b: Urban Dust, National Institute of Standards & Technology, Gaithersburg, MD, 14 pp., 2009.

Yttri, K. E., Dye, C., and Kiss, G.: Ambient aerosol concentrations of sugars and sugar-alcohols at four different sites in Norway, At-

mos. Chem. Phys., 7, 4267–4279, doi:10.5194/acp-7-4267-2007, 2007.

Zhang, Y. L., Perron, N., Ciobanu, V. G., Zotter, P., Minguillón, M. C., Wacker, L., Prévôt, A. S. H., Baltensperger, U., and Szidat, S.: On the isolation of OC and EC and the optimal strategy of radiocarbon-based source apportionment of carbonaceous aerosols, Atmos. Chem. Phys., 12, 10841–10856, doi:10.5194/acp-12-10841-2012, 2012.

Zotter, P., Ciobanu, V. G., Zhang, Y. L., El-Haddad, I., Macchia, M., Daellenbach, K. R., Salazar, G. A., Huang, R.-J., Wacker, L., Hueglin, C., Piazzalunga, A., Fermo, P., Schwikowski, M., Baltensperger, U., Szidat, S., and Prévôt, A. S. H.: Radiocarbon analysis of elemental and organic carbon in Switzerland during winter-smog episodes from 2008 to 2012 – Part 1: Source apportionment and spatial variability, Atmos. Chem. Phys., 14, 13551–13570, doi:10.5194/acp-14-13551-2014, 2014.